



Oude Waalsdorperweg 63
P.O. Box 96864
2509 JG The Hague
The Netherlands

www.tno.nl

T +31 70 374 00 00
F +31 70 328 09 61
info-DenV@tno.nl

TNO report

TNO-DV 2006 A518

Algorithms for the fusion of two sets of (sonar)
data

Date December 2006
Author(s) dr P.A.M. de Theije
C.A.M. van Moll, MSc

Classification report Ongerubriceerd
Classified by E. van der Spek, BS
Classification date 19-12-2006

Title Ongerubriceerd
Managementuittreksel Ongerubriceerd
Abstract Ongerubriceerd
Report text Ongerubriceerd
Appendices Ongerubriceerd

20070813231

Copy no 6
No. of copies 18
Number of pages 51 (incl. appendices, excl. RDP & distributionlist)
Number of appendices 0

The classification designation Ongerubriceerd is equivalent to Unclassified, Stg. Confidentieel is equivalent to Confidential and Stg. Geheim is equivalent to Secret.

All rights reserved. No part of this report may be reproduced in any form by print, photoprint, microfilm or any other means without the previous written permission from TNO.

All information which is classified according to Dutch regulations shall be treated by the recipient in the same way as classified information of corresponding value in his own country. No part of this information will be disclosed to any third party.

In case this report was drafted on instructions from the Ministry of Defence the rights and obligations of the principal and TNO are subject to the standard conditions for research and development instructions, established by the Ministry of Defence and TNO, if these conditions are declared applicable, or the relevant agreement concluded between the contracting parties.

© 2006 TNO

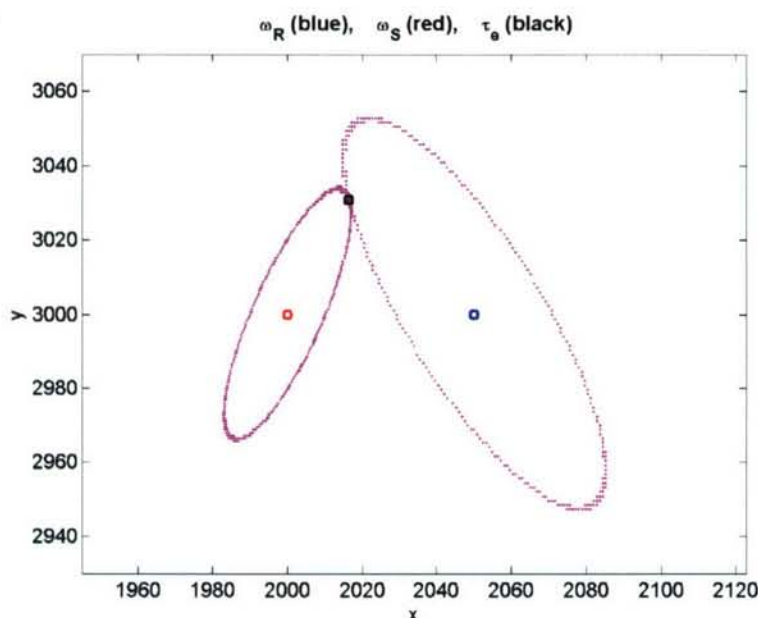
DISTRIBUTION STATEMENT A

Approved for Public Release
Distribution Unlimited

AQ F07-11-12014

Algoritmes voor het fuseren van twee sets (sonar) data

Bij het combineren van meerdere sensoren is het belangrijk de informatie van de verschillende sensoren zo goed mogelijk samen te voegen. Dit kan grote impact hebben op de prestatie van het gecombineerde systeem. In dit rapport worden verschillende manieren onderzocht om de informatie van de verschillende sensoren (in ons geval sonars) te combineren.



Probleemstelling

Een groot deel van het programma 'Onderzeewaterbeeldopbouw in ondiep water' (V506) is gericht op onderzoek op het gebied van multistatische operaties. De Koninklijke Marine heeft hier interesse in omdat dergelijke operaties komende jaren zowel nationaal als internationaal een steeds belangrijkere rol zullen gaan spelen tijdens onderzeebootbestrijdingsoperaties. Bij multistatische operaties worden sonars

van meerdere platformen tegelijk ingezet, wat grote tactische voordelen kan hebben en een verbeterde prestatie belooft. Voor een optimale prestatie in een multistatische operatie dient de verkregen informatie van alle sonars naar een centraal punt gestuurd te worden, waar het gefuseerd kan worden. In dit rapport wordt het probleem van de fusie van (sonar)data besproken, in de aanwezigheid van fouten op de posities van geïdentificeerde (sonar)contacten.

De contacten zijn over het algemeen van verschillende sonarsystemen afkomstig en worden meestal niet op precies de goede positie waargenomen. Hoe kunnen deze optimaal worden gecombineerd om een zo groot mogelijke prestatie of prestatieverbetering ten opzichte van de individuele sonars te hebben?

Resultaten en conclusies

Uit de theorie volgt dat de positie van een contact na fusie significant anders kan zijn dan de positie van de oorspronkelijke contacten waaruit het is voortgekomen. Deze positie na fusie ligt, tegen de verwachting in, meestal niet op de verbindingslijn tussen de twee oorspronkelijke objecten.

De detectieprestatie, na samenvoegen van de doelcontacten en loosalarmen van twee sonars, verbetert aanzienlijk, met 1 tot 5 dB. Daadwerkelijk fuseren van de twee sets contacten (dat wil zeggen, in de samengevoegde set de contacten die 'dicht genoeg bij elkaar liggen' combineren in één nieuw contact) voegt hier geen verbetering aan toe in termen van detectieprestatie.

Enkele van de onderzochte fusie-algoritmes laten echter wel een verbeterde positiebepaling van de gefuseerde contacten zien ten opzichte van die van de originele contacten. Dit kan belangrijk zijn als deze contacten bijvoorbeeld aan een trackingalgoritme worden gevoed, aangezien de prestatie van een dergelijk algoritme sterk afhangt van nauwkeurige positie-informatie van de invoer.

Toepasbaarheid

De beschreven fusie-algoritmes kunnen in de bestaande (IR)LFAS-signaalverwerkingsketen ingebouwd worden. Als er dan multistatische operaties worden uitgevoerd met het (IR)LFAS-systeem kunnen de algoritmes een gewenste tussenstap vormen alvorens alle sonarcontacten aan een trackingalgoritme te voeren.

PROGRAMMA	PROJECT
Programmabegeleider ing. E. van de spek, DMO/DWS&B/RZS&B	Projectbegeleider ing. E. van de spek, DMO/DWS&B/RZS&B
Programmaleider dr. S.P. Beerens, TNO Defensie en Veiligheid	Projectleider dr. P.A.M. de Theije, TNO Defensie en Veiligheid
Programmatitel Onderwaterbeeldopbouw in ondiep water	Projecttitel LFAS netcentric
Programmanummer V506	Projectnummer 015.34675
Programmaplanning Start 01-01-2005 Gereed 31-12-2008	Projectplanning Start 01-01-2005 Gereed 31-12-2008
Toezichthouder -	
Frequentie van overleg Met de programma/projectbegeleider werd eens per kwartaal gesproken over de invulling en de voortgang van het onderzoek.	Projectteam dr. P.A.M. de Theije, ir. C.A.M. van Moll

Contact en rapportinformatie

Oude Waalsdorperweg 63
Postbus 96864
2509 JG Den Haag

T +31 70 374 00 00
F +31 70 328 09 61

info-DenV@tno.nl

TNO-rapportnummer
TNO-DV 2006 A518

Opdrachtnummer
-

Datum
december 2006

Auteur(s)
dr. P.A.M. de Theije
ir. C.A.M. van Moll

Rubricering rapport
Ongerubriceerd

Abbreviations

JRP	Joint Research Project
ML	Maximum Likelihood (estimate)
NURC	NATO Undersea Research Centre
pdf	probability density function
ROC	Receiver Operating Curves
SNR	Signal-to-Noise Ratio
TNO	Netherlands Organisation for Applied Scientific Research
TNO-DenV	TNO Defence, Security and Safety

List of symbols

Theory, general

$N(\mu, \sigma^2)$	Normal distribution with mean μ and variance σ^2
R	Receiver system 1
S	Receiver system 2
$P\{A_1 \vee A_2\}$	Probability of event A_1 or A_2
$P\{A_1 \wedge A_2 B\}$	Probability of event A_1 and A_2 under the condition of event B
$P\{a \notin A\}$	Probability of event that a is not an element of the set A
$E\{x\}$	Expected value of the statistic x

Theory, one-dimensional case

T	True target position
T_e	Stochastic variable of target position
τ_e	ML estimate of target position
W_R	Stochastic variable of position of detection by receiver R
ω_R	Observation of W_R
σ_R	Standard deviation of W_R
W_S	Stochastic variable of position of detection by receiver S
ω_S	Observation of W_S
σ_S	Standard deviation of W_S

Theory, two-dimensional case

$T = (x_T, y_T)$	True target position
T_e	Stochastic variable of target position
$\tau_e = (\tau_X, \tau_Y)$	ML estimate of target position
W_R	Stochastic variable of position of detection by receiver R
$\omega_R = (x_R, y_R)$	Observation of W_R
C_R	Covariance matrix of W_R
W_S	Stochastic variable of position of detection by receiver S
$\omega_S = (x_S, y_S)$	Observation of W_S
C_S	Covariance matrix of W_S

List of symbols (continued)

Simulations

c	Sound speed in water [m/s]
$(x_{s,i}, y_{s,i})$	(x , y)-position sonar i ($i = 1,2$) [m]
$(\Delta x_{s,i}, \Delta y_{s,i}, \sigma_{xy,s,i})$	Error in (x , y)-position sonar i [m]
$\Delta \theta_i$	Error in receiver heading sonar i [deg]
$\Delta \varphi_i$	Error in bearing estimate with sonar i [deg]
Δt_i	Time-synchronisation accuracy sonar i [s]
$SNR_{j,i}$	Target signal-to-noise ratio of target j relative to sonar i [dB]
$(x_{t,i}, y_{t,i})$	(x , y)-position of target as observed by sonar i [m]
A_T	Amplitude threshold [dB]
ΔA_T	Increase in amplitude threshold [dB] due to data fusion
$N_{d,i,p}(A_T)$	Number of detections by sonar i for ping p
$N_{fa,i,p}(A_T)$	Number of false alarms by sonar i for ping p
$p_{d,i}(A_T)$	Probability of detection by sonar i
$p_{fa,i}(A_T)$	Probability of false alarm by sonar i
C_i	Set of threshold crossings from sonar i

Summary

In this report we have focussed on the topic of multistatic sensor and data fusion. First, we have established a theoretical foundation for the probability that two contacts, as observed by two separate systems, are due to the same target. This derivation includes the position errors in the observations that are expected for both systems. Apart from the association probability, the most-likely target position is obtained. The theory is derived for the one- and two-dimensional cases.

To test the above theory, and to assess the benefit of data fusion, realistic simulations have been carried out. These simulations are based mainly on common Rayleigh statistics, both for the background and the target amplitudes. They take into account position errors in the observations (to mimic the fact that any sensor will not yield infinitely accurate contact positions), finite sampling (in time and bearing) of the sonars, and can include targets of different signal-to-noise ratios and at different positions.

The following definitions are used throughout the report:

- ‘Combining’: All contacts identified by the two separate systems are stored in a single set of contacts.
- ‘Fusing’: As in ‘combining’, but for each pair of contacts from both systems it is checked if they originate from the same target. If so, this pair of contacts is merged into a single contact.
- ‘OR’ fusing: All contacts that have formed after ‘fusing’ are taken into account.
- ‘AND’ fusing: Only those contacts that have formed after ‘fusing’ and that originate from two contacts, one from each system, are taken into account.

The main conclusions from the simulations are as follows:

- Combining two data sets of independent sonars, the total detection performance of the system improves significantly in comparison to a single sonar. This is due to the enhanced probability of detection, despite the increase (by a factor of two) of the number of false alarms.
- Fusing the two data sets with the ‘OR’ rule, the total detection performance (as evaluated from the ROC curves) of the system is equal to the (improved) performance of the combined system. Although it was expected that fusing two data sets would give a better performance than combining them, this is not the case.
- Fusing the two data sets with the ‘AND’ rule, the total detection performance of the system decreases relative to that of the single sonars. The reason for this decrease is the inaccurate positions of the original contacts, which cause only few pairs of target-originated contacts to actually fuse. Without position errors included, it has been shown by others that the performance after ‘AND’ fusion would be equal to that of the original sonars.
- After ‘OR’ fusion, the standard deviations of the observed contact-position errors decrease with threshold A_T , especially at higher thresholds, $A_T > 16$ dB. The standard deviations have roughly reduced to one third of their original value between $A_T = 10$ and $A_T = 20$ dB. This is because at higher threshold relatively more fused contacts are present, that have a higher position accuracy.

- After 'AND' fusion, the standard deviations of the observed contact-position errors also decreases with threshold A_T , the decrease being more profound at lower values of A_T than after 'OR' fusion.

The following conclusions from the simulations hold for all fusion algorithms:

- Applying a small increase in the threshold ΔA_T as part of the fusion algorithm, results in a slightly lower ROC curve and is therefore not a good idea.
- The performance results of the different fusion algorithms do not change noticeably with the number of targets in the simulations, at least in the range 1 – 30.
- For high mean target SNR (≈ 20 dB), some fusion algorithms show relatively high false-alarm probabilities at high amplitude thresholds ($A_T > 16$ dB), due to the fusion of target-originated contacts and false contacts.
- A single simulation, where the target-amplitude follows a one-dominant-plus-Rayleigh distribution rather than a Rayleigh distribution, suggests that the results quoted above do not depend very much on the target-amplitude distribution.

The above results indicate that combining or 'OR'-fusing two datasets gives a considerable increase in performances in comparison to a single sonar.

However, 'AND' fusion is not a good option in terms of detection performance, especially not in the case of large contact-position errors. 'OR' fusion does not add detection performance (compared to just combining the two data sets), but it does yield more accurate position information to the fused data set. This can be important if the resulting data sets are fed to a tracking algorithm, especially in heavy cluster areas, where many contacts may occur in a small volume.

Contents

	Managementuittreksel	2
	Abbreviations	4
	List of symbols	5
	Summary	7
1	Introduction	10
1.1	Background.....	10
1.2	Motivation for current research.....	10
1.3	Outline of report	11
2	Theoretical analysis	12
2.1	Statistical concepts.....	12
2.2	One dimensional case	12
2.3	Two-dimensional case	15
3	Understanding the association probability.....	21
3.1	Visual presentation of the association probability	21
3.2	Practical way to calculate the association probability.....	22
3.3	Analysis of association probability	23
4	Performance estimation by means of simulations.....	25
4.1	Introduction	25
4.2	Simulations	25
4.3	Parameters of simulation scenario.....	29
4.4	Single-sonar results.....	30
4.5	Statistics of fusions	34
4.6	Increase in amplitude threshold after fusion.....	38
4.7	False-alarm probability after fusion	39
4.8	Probability of detection after fusion	41
4.9	ROC curves after fusion.....	42
4.10	ROC curves for different simulation parameters	44
4.11	Improvement in localisation after fusion.....	47
5	References	50
6	Signature	51

1 Introduction

1.1 Background

Multistatic operations can have great advantages: they can lead to larger detection ranges and a better coverage of a possible submarine operations area. Also, such operations can be less dangerous for the participating units as only one source is needed and all other units can operate passively and thus remain covert. Apart from tactical advantages, also acoustical advantages may be obtained (e.g. less reverberation). In addition, significant gain is expected from the combination of mono- and bistatic detections. Combining the information of multiple (either monostatic or bistatic) sonar systems should in theory provide enhanced detection performance, more clues towards classification [2], and increased localization accuracy. For the latter, positioning issues play an important role. In [1] [3] [4] it was shown that the uncertainty of the position of a detection by a receiver depends in general on the errors in:

- Sound speed.
- Receiver heading.
- Bearing estimate.
- Accuracy of time of reception.
- Source- and receiver-position errors.

The combined effect of all these components can, in some cases, generate quite large uncertainties in the target-contact position, up to several hundred metres.

The relative importance of these parameters depends on the target position itself, and on the receiver being monostatic or bistatic.

For an overview of the current status of multistatic research, see the excellent overview in [5].

1.2 Motivation for current research

The current research is carried out in the context of the project 'LFAS Netcentric', part of the programme 'Onderzeebootbestrijdingscapaciteit in ondiep water'.

The main themes of this project are:

- 1 Data fusion.
- 2 Multi-sensor target tracking.
- 3 Including submarine sensors in multistatic operations.
- 4 Netcentric underwater communication.
- 5 Including dipping sonars and sonobuoys in multistatic operations.

This report focuses on the first theme: Data fusion.

Trying to fuse two data sets, originating from different receivers, one has to deal with the position errors as target contacts are in general not perfectly aligned.

The question that arises then is: *How to combine in an optimal way the contacts from the different receivers?* This question is relevant, e.g., for multistatic tracking algorithms: if multiple sonar systems are executing a joint operation, their identified sonar contacts can be combined and fed to a so-called centralised tracker.

This tracker receives all sonar contacts of all sonars and from these tries to form

consistent tracks by associating contacts at different time stamps. For such algorithms the quality of the input is very important: the position accuracy of the input contacts should be as good as possible, and the number of input contacts should not be too large. For both purposes it is important to combine the contacts of the different sonars optimally.

1.3 Outline of report

This report is organised as follows: Chapter 2 describes the theory of how to associate two contacts, as observed by two sonar receivers. This gives an association probability for these contacts to be due to the same target, as well as a most-likely position of the combined contact. In Chapter 3 this theory is illustrated using a simple example. Chapter 4 presents the simulations that are used to assess the performance of the data-association algorithms, as well as an evaluation of the improvements to be expected due to data association.

2 Theoretical analysis

2.1 Statistical concepts

Consider a sonar system with two independent observation systems: one receiver S, and a second receiver R. For example, for a simple bistatic system, S can be collocated with the source position, while R is assumed to be at a certain distance from the source. However, the exact operating mode of S and R does not change the algorithms below. A signal transmitted by the source reflects on the target and may cause a contact by each of the two independent observation systems. The position \mathbf{W}_S of the contact by receiver S is assumed to be a normally distributed stochastic variable, centred at the target position \mathbf{T} with its (co)variance \mathbf{C}_S determined by this position. The position \mathbf{W}_R of the contact by R has its own normal distribution, also centred at the target position but with (co)variance \mathbf{C}_R . That is,

$$\mathbf{W}_S \sim N(\mathbf{T}, \mathbf{C}_S) \quad \text{and} \quad \mathbf{W}_R \sim N(\mathbf{T}, \mathbf{C}_R)$$

with $N(\boldsymbol{\mu}, \mathbf{C})$ representing a normal distribution with mean $\boldsymbol{\mu}$ and (co)variance \mathbf{C} . Since both contacts are assumed independent, the probability density function (pdf) for a combination of both contacts is the product of their individual probability density functions. However, given the event of combined detected positions $(\boldsymbol{\omega}_S, \boldsymbol{\omega}_R)$ which come from the same target, this target position \mathbf{T} is unknown and must be estimated from this given combination. This can be realised with the concept of the maximum likelihood (ML) estimator, by estimating the target position \mathbf{T} by that value $\boldsymbol{\tau}_e$ that maximises the probability density of the $(\boldsymbol{\omega}_S, \boldsymbol{\omega}_R)$ -combination.

For any event of combined detected positions $(\boldsymbol{\omega}_S, \boldsymbol{\omega}_R)$ – no matter how far apart – an estimated target position $\boldsymbol{\tau}_e$ can be calculated in this way. The question remains how likely it is that both contacts result from the same target. This can be addressed by calculating the total probability of combinations $(\mathbf{W}_S, \mathbf{W}_R)$ that are equally or less likely than the actual observed combination $(\boldsymbol{\omega}_S, \boldsymbol{\omega}_R)$, assuming that they represent the same target at the estimated position $\boldsymbol{\tau}_e$.

Both concepts – the maximum likelihood estimate of the target position and the probability of the observed contact combination – will be applied first in a one-dimensional space to increase our understanding. Thereafter they will be implemented for two-dimensional localisation in the plane.

2.2 One dimensional case

2.2.1 Probability-density functions

Suppose the target has to follow a very narrow sea lane. As a result the detection problem becomes one dimensional, making the analysis rather simple. The position of the contact W_S by receiver S and of the contact W_R of receiver R are independent normally-distributed stochastic variables, both centred at the target position T but each with their own variances, σ_S^2 and σ_R^2 respectively.

That is,

$$W_S \sim N(T, \sigma_S^2)$$

and

$$W_R \sim N(T, \sigma_R^2)$$

The probability-density function (pdf) for the observed combination of contacts (ω_S, ω_R) becomes

$$p(\omega_S, \omega_R) = p(\omega_S)p(\omega_R) = \frac{1}{2\pi\sigma_S\sigma_R} \exp\left(-\frac{1}{2}A\right) \quad (3.1)$$

with

$$A = \left(\frac{\omega_S - T}{\sigma_S}\right)^2 + \left(\frac{\omega_R - T}{\sigma_R}\right)^2 \quad (3.2)$$

Remark that W_S and W_R are stochastic variables, while ω_S and ω_R represent observed values.

2.2.2 Maximum-likelihood target position

For a given realisation (ω_S, ω_R) the value of $p(\omega_S, \omega_R)$ in Equation (3.1) depends on the (unknown) true target position T . Maximising $p(\omega_S, \omega_R)$ by varying T is equivalent to minimising A . This is realised if T is equal to τ_e , the ML estimate for the target position, which is obtained by differentiating Equation (3.2) and is given by

$$\tau_e = \left(\frac{\sigma_S^2}{\sigma_S^2 + \sigma_R^2}\right)\omega_R + \left(\frac{\sigma_R^2}{\sigma_S^2 + \sigma_R^2}\right)\omega_S \quad (3.3)$$

τ_e is thus a linear combination of the observed contact positions ω_S and ω_R and is closest to the observation with the smallest variance.

2.2.3 Probability of contact association

Derivation of the probability of association is slightly more demanding. It is equal to the probability of combinations of contact positions (W_S, W_R) that are equally or less likely than the actually observed combination (ω_S, ω_R) , under the assumption that the distributions of the contacts W_S and W_R are both centered at τ_e . In the following we assume that $\omega_R \geq \omega_S$, but in case $\omega_R < \omega_S$ a similar reasoning can be followed.

To work out the consequences of the assumption that $T = \tau_e$, we define the stochastic variable T_e as follows

$$T_e = \left(\frac{\sigma_S^2}{\sigma_S^2 + \sigma_R^2}\right)W_R + \left(\frac{\sigma_R^2}{\sigma_S^2 + \sigma_R^2}\right)W_S \quad (3.4)$$

τ_e , the ML estimate for T , is derived from the contact event (ω_S, ω_R) and therefore is the outcome of a stochastic process. Taking this outcome serious imposes a restriction on the stochastic contact combinations (W_S, W_R) taken into consideration to determine the association probability. Only those combinations are allowed that yield the same value τ_e for T . The assumption is thereby transformed into the condition $T_e = \tau_e$, imposing a relation between the stochastic variables W_S and W_R .

With this, the probability of contact association P_{ass} becomes equal to the total probability of combinations of contact positions (W_S, W_R) that are equally or less likely than the actually observed combination (ω_S, ω_R) , under the condition that $T_e = \tau_e$:¹

$$P_{ass} = P\{W_R \geq \omega_R \wedge W_S \leq \omega_S \mid T_e = \tau_e\} = \frac{P\{W_R \geq \omega_R \wedge W_S \leq \omega_S \wedge T_e = \tau_e\}}{P\{T_e = \tau_e\}} \quad (3.5)$$

$T_e = \tau_e$ imposes the following restriction on the (W_S, W_R) combinations:

$$\tau_e = \left(\frac{\sigma_S^2}{\sigma_S^2 + \sigma_R^2} \right) W_R + \left(\frac{\sigma_R^2}{\sigma_S^2 + \sigma_R^2} \right) W_S \quad (3.6)$$

Only combinations of W_S and W_R that satisfy this relation can result in the estimated target position. Therefore W_S is linked to W_R via

$$W_S = \frac{(\sigma_S^2 + \sigma_R^2)\tau_e - \sigma_S^2 W_R}{\sigma_R^2} \quad (3.7)$$

Consequently

$$P\{W_R \geq \omega_R \wedge W_S \leq \omega_S \wedge T_e = \tau_e\} = P\left\{W_R \geq \omega_R \wedge W_S = \frac{(\sigma_S^2 + \sigma_R^2)\tau_e - \sigma_S^2 W_R}{\sigma_R^2}\right\} \quad (3.8)$$

and

$$P\{T_e = \tau_e\} = P\left\{W_R \geq \tau_e \wedge W_S = \frac{(\sigma_S^2 + \sigma_R^2)\tau_e - \sigma_S^2 W_R}{\sigma_R^2}\right\} \quad (3.9)$$

Substituting Equation (3.7) for W_S into Formula (3.1) for $p(W_S, W_R)$ and integrating over $W_R \geq \omega_R$ and over $W_R \geq \tau_e$, finally gives the probability of association of the observed combination (ω_S, ω_R) :

$$P_{ass} = 1 - \text{erf}\left(\frac{\omega_R - \omega_S}{\sqrt{2\sigma_S^2 + 2\sigma_R^2}}\right) \quad (3.10)$$

where $\text{erf}(\cdot)$ denotes the error function, and the argument of the error function is equal to the so-called Mahalanobis distance between ω_R and ω_S . In fact, it can be shown that if (W_S, W_R) are randomly drawn from $W_S \sim N(T_e, \sigma_S^2)$ and $W_R \sim N(T_e, \sigma_R^2)$, respectively, then P_{ass} , as given in (3.10) is equal to the fraction of such (W_S, W_R) combinations that are more distant from each other than $|\omega_S - \omega_R|$.

Figure 2.1 shows the effect of an increasing distance between the observed contacts on their association probability. We will give some numerical examples later on in Table 2.1.

¹ The notation is given in the list of symbols, under 'theory general'.

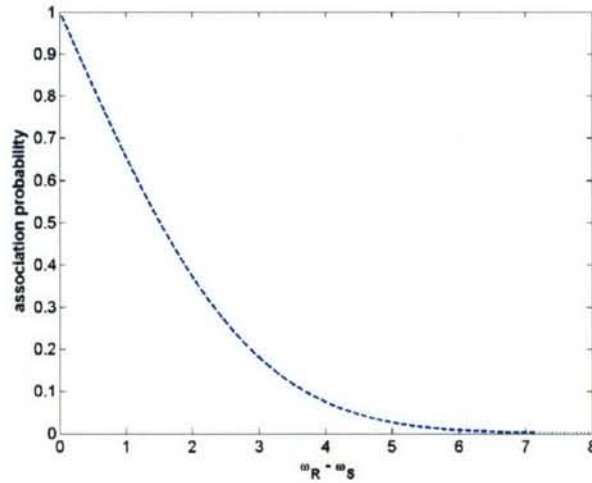


Figure 2.1 Association probability versus distance $\omega_R - \omega_S$ between two observations ω_R and ω_S , in case $\sigma_S = 1$ and $\sigma_R = 2$.

2.3 Two-dimensional case

In the case the target is located in a two-dimensional plane, the target position \mathbf{T} , and the contact position \mathbf{W}_S and \mathbf{W}_R all have two coordinates. We introduce the following notation

$$\mathbf{W}_S = (x_S, y_S) \quad \mathbf{W}_R = (x_R, y_R) \quad \text{and} \quad \mathbf{T} = (x_T, y_T)$$

In this case the probability distributions of the two detection devices become bivariate normal distributions, both centred at the target position \mathbf{T} , but with their own covariance matrices, \mathbf{C}_S resp. \mathbf{C}_R , i.e.

$$\mathbf{W}_S \sim N(\mathbf{T}, \mathbf{C}_S) \quad \text{and} \quad \mathbf{W}_R \sim N(\mathbf{T}, \mathbf{C}_R)$$

This looks rather complicated, but it is not if it is presented in a proper way. Therefore we first present multivariate normal distributions and then go back to the simpler bivariate case.

2.3.1 Intermezzo: Multivariate normal distribution

Suppose \mathbf{v} is an n -dimensional vector with an n -variate normal distribution. Then the pdf of $\mathbf{v} = (v_1, v_2, \dots, v_n)^T$ is

$$p(\mathbf{v}) = \frac{1}{\sqrt{(2\pi)^n \text{Det}(\mathbf{C}_v)}} \exp\left(-\frac{1}{2}(\mathbf{v} - \boldsymbol{\mu}_v)^T \mathbf{C}_v^{-1} (\mathbf{v} - \boldsymbol{\mu}_v)\right) \quad (3.11)$$

with $\boldsymbol{\mu}_v$ the vector of expected values of \mathbf{v} , \mathbf{C}_v the covariance matrix of \mathbf{v}

$$\mathbf{C}_v = \begin{bmatrix} \sigma_{11} & \sigma_{12} & \dots & \sigma_{1n} \\ \sigma_{21} & \sigma_{22} & \dots & \sigma_{2n} \\ \dots & \dots & \dots & \dots \\ \sigma_{n1} & \sigma_{n2} & \dots & \sigma_{nn} \end{bmatrix}$$

with

$$\sigma_{km} = E\left\{\left(v_k - \mu_{v_k}\right)^T \left(v_m - \mu_{v_m}\right)\right\} = \sigma_{mk}$$

and $\text{Det}(\mathbf{C}_v)$ the determinant of \mathbf{C}_v .

We define

$$\sigma_k = \sqrt{\sigma_{kk}}$$

and

$$\rho_{km} = \frac{\sigma_{km}}{\sigma_k \sigma_m}$$

For the case $n = 1$ the well-known pdf of the one-dimensional normal distribution results.

2.3.2 Probability-density functions

The positions \mathbf{W}_S detected by receiver S have the following bivariate normal distribution ($n = 2$):

$$(x_S, y_S) \sim N((x_T, y_T), \mathbf{C}_S)$$

with

$$\mathbf{C}_S = \begin{pmatrix} \sigma_1^2 & \sigma_{12} \\ \sigma_{21} & \sigma_2^2 \end{pmatrix} = \begin{pmatrix} \sigma_{XS}^2 & \rho_S \sigma_{XS} \sigma_{YS} \\ \rho_S \sigma_{XS} \sigma_{YS} & \sigma_{YS}^2 \end{pmatrix}$$

There is a change in notation here: the dimensions 1 and 2 are relabelled by X and Y respectively.

Inserting the covariance matrix \mathbf{C}_S into the pdf-Formula (3.11) results in

$$p(\omega_S) = p(x_S, y_S) = \frac{1}{2\pi\sigma_{XS}\sigma_{YS}\sqrt{1-\rho_S^2}} \exp\left(-\frac{1}{2}A_S\right) \quad (3.12)$$

with

$$A_S = \frac{1}{(1-\rho_S^2)} \left[\left(\frac{x_S - x_T}{\sigma_{XS}} \right)^2 - 2\rho_S \left(\frac{x_S - x_T}{\sigma_{XS}} \right) \left(\frac{y_S - y_T}{\sigma_{YS}} \right) + \left(\frac{y_S - y_T}{\sigma_{YS}} \right)^2 \right] \quad (3.13)$$

For the positions \mathbf{W}_R observed by receiver R each subscript 'S' must be replaced by an 'R'. Since the stochastic contact positions \mathbf{W}_S and \mathbf{W}_R are assumed to be independent, the pdf for a combination of both contacts is the product of their individual pdf's.

For the measurement $(\omega_S, \omega_R) = ((x_S, y_S), (x_R, y_R))$ the probability density becomes

$$p(x_S, y_S, x_R, y_R) = \frac{1}{2\pi\sigma_{XS}\sigma_{YS}\sqrt{1-\rho_S^2}} \frac{1}{2\pi\sigma_{XR}\sigma_{YR}\sqrt{1-\rho_R^2}} \exp\left(-\frac{1}{2}(A_S + A_R)\right) \quad (3.14)$$

Remark that the assumption that both contacts come from the same target is already incorporated in the $A = A_S + A_R$ part of this formula. The target position (x_T, y_T) , however, is yet unknown and must be estimated.

2.3.3 Maximum-likelihood target position

For a given combination (ω_S, ω_R) the value of $p(\omega_S, \omega_R)$ depends on $\mathbf{T} = (x_T, y_T)$. Maximising $p(\omega_S, \omega_R)$ by varying \mathbf{T} is equal to minimising A . Making both partial derivatives of A with respect to x_T and y_T equal to zero, results in the ML estimate for the target position $\tau_e = (\tau_x, \tau_y)$, which can be shown to be equal to

$$\tau_e = \omega_S + \mathbf{M} \cdot (\omega_R - \omega_S) \quad (3.15)$$

with

$$\mathbf{M} = \begin{pmatrix} \alpha & \gamma \\ \delta & \beta \end{pmatrix} \quad (3.16)$$

and

$$\alpha = \frac{\sigma_{XS}^2 \sigma_{YS}^2 (\rho_S^2 - 1) - \sigma_{XS}^2 \sigma_{YR}^2 + \rho_R \rho_S \sigma_{XS} \sigma_{YS} \sigma_{XR} \sigma_{YR}}{B}$$

$$\beta = \frac{\sigma_{XS}^2 \sigma_{YS}^2 (\rho_S^2 - 1) - \sigma_{XR}^2 \sigma_{YS}^2 + \rho_R \rho_S \sigma_{XS} \sigma_{YS} \sigma_{XR} \sigma_{YR}}{B}$$

$$\gamma = \frac{\rho_R \sigma_{XR} \sigma_{YR} \sigma_{XS}^2 - \rho_S \sigma_{XS} \sigma_{YS} \sigma_{XR}^2}{B}$$

$$\delta = \frac{\rho_R \sigma_{XR} \sigma_{YR} \sigma_{YS}^2 - \rho_S \sigma_{XS} \sigma_{YS} \sigma_{YR}^2}{B}$$

$$B = \sigma_{XS}^2 \sigma_{YS}^2 (\rho_S^2 - 1) + \sigma_{XR}^2 \sigma_{YR}^2 (\rho_R^2 - 1) - \sigma_{XS}^2 \sigma_{YR}^2 - \sigma_{XR}^2 \sigma_{YS}^2 + 2\rho_S \rho_R \sigma_{XS} \sigma_{YS} \sigma_{XR} \sigma_{YR}$$

Usually τ_e will not just be a linear combination of the observed contact positions ω_S and ω_R , because $\mathbf{M} \neq \alpha \mathbf{I}$. If $\alpha = \beta$ and $\gamma = \delta = 0$, (τ_x, τ_y) will be on the line between (x_S, y_S) and (x_R, y_R) . In this case

$$\frac{\sigma_{XS}}{\sigma_{YS}} = \frac{\sigma_{XR}}{\sigma_{YR}} \quad \text{and} \quad \rho_S = \rho_R$$

and the pdf-contours of \mathbf{W}_S and \mathbf{W}_R will have exactly the same shape and orientation, but can have a different scaling factor. This is demonstrated in the upper panels of Figure 2.2, where the target position is on the line between the two observed contacts. The fact that the ML estimate of the target position τ_e is usually not on the line between the two observed contact positions ω_S and ω_R , is an unexpected result that is important for target localisation. This is illustrated in the lower panels of Figure 2.2. By plotting the probability density contours of the contacts, these panels give an impression of how the probability distributions of \mathbf{W}_S and \mathbf{W}_R can influence the ML target position. In Table 2.1 the input and output of Figure 2.2 is presented numerically. Note that, in each panel, the contours shown for ω_S and ω_R do in general not correspond to the same pdf-value, but are the ones that pass through τ_e .

Table 2.1 Numerical inputs and outputs used to generate the four panels of Figure 2.2 (arbitrary units).

	upper left	upper right	lower left	lower right
input				
x_S	2000	2000	2000	2000
y_S	3000	3000	3000	3000
σ_{xS}	15	15	20	20
σ_{yS}	20	20	40	40
ρ_S	0.4	0.8	0.4	0.8
x_R	2030	2030	2050	2050
y_R	2960	2960	3000	3000
σ_{xR}	30	30	40	40
σ_{yR}	40	40	60	60
ρ_R	0.4	0.8	-0.4	-0.8
output				
x_T	2006	2006	2011.4	2016.5
y_T	2992	2992	3013.5	3030.7
association probability	0.24	0.02	0.59	0.60
α	0.2	0.2	0.23	0.33
β	0.2	0.2	0.34	0.46
γ	0	0	0.09	0.20
δ	0	0	0.27	0.61

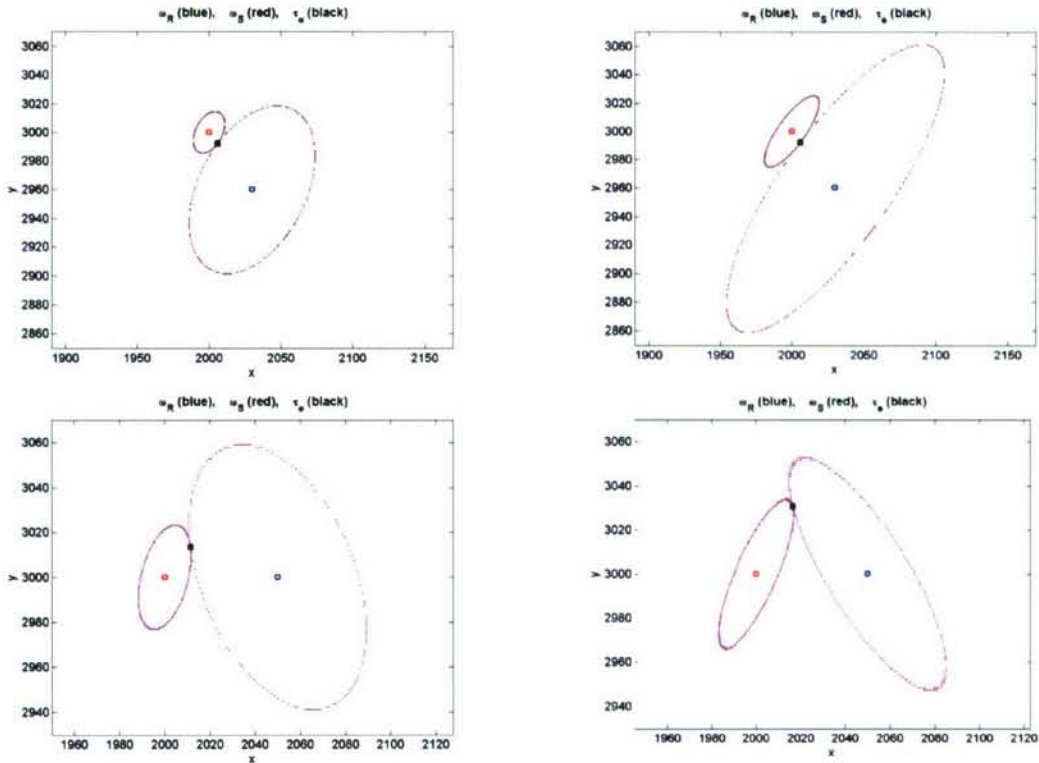


Figure 2.2 Example pdf contours of contact positions W_S and W_R centred at w_S (red dot) and w_R (blue dot), with maximum likelihood target position τ_e (black dot). Upper panels: target τ_e on line between w_S and w_R ; lower panels: target τ_e not on the line between w_S and w_R . Parameter values given in Table 2.1.

2.3.4 Probability of contact association

As in the one-dimensional case, the probability of association is set equal to the likelihood of getting the observed contact positions ω_S and ω_R (or less likely values) from the distributions of W_S and W_R , under the assumption that these distributions are both centred at τ_e . Let us define the stochastic variable T_e as

$$T_e = W_S + M \cdot (W_R - W_S) \quad (3.17)$$

Following the same reasoning as in the one-dimensional case, the assumption that $T = \tau_e$ is transformed into the condition $T_e = \tau_e$, which imposes the restriction on the stochastic contact combination (W_S, W_R) that each combination should yield the same ML estimate τ_e for T as the observed combination (ω_S, ω_R) does.

With this the probability of contact association becomes equal to the total probability of combinations of contact positions (W_S, W_R) which are equally or less likely than the actually observed combination (ω_S, ω_R) under the condition that $T_e = \tau_e$.

In the two-dimensional case, however, the definition of “less likely” has to be adjusted. Here we call positions W_S less likely than the observed value ω_S if $\text{pdf}_S(W_S) \leq \text{pdf}_S(\omega_S)$, with $\text{pdf}_S(\omega_S)$ the probability density at ω_S . So less likely positions W_S are all points outside the probability density contour going through ω_S , which can be shown to be an ellipse. We denote all vectors inside this ellipse by $E(\omega_S)$. The same can be done for the R system, by replacing all subscripts ‘S’ by ‘R’.

With all this background the association probability P_{ass} is defined as

$$P_{ass} = P\{W_R \notin E(\omega_R) \vee W_S \notin E(\omega_S) \mid T_e = \tau_e\} = 1 - \frac{P\{W_R \in E(\omega_R) \wedge W_S \in E(\omega_S) \wedge T_e = \tau_e\}}{P\{T_e = \tau_e\}} \quad (3.18)$$

The condition $T_e = \tau_e$ is equivalent to the following expression for W_S

$$W_S = (I - M)^{-1} \cdot (\tau_e - M \cdot W_R) \quad (3.19)$$

With this we get

$$P\{W_R \in E(\omega_R) \wedge W_S \in E(\omega_S) \wedge T_e = \tau_e\} = P\{W_R \in E(\omega_R) \wedge W_S \in E(\omega_S) \wedge W_S = (I - M)^{-1} \cdot (\tau_e - M \cdot W_R)\}$$

and

$$P\{T = \tau_e\} = P\{W_R \in \mathbf{R}^2 \wedge W_S = (I - M)^{-1} \cdot (\tau_e - M \cdot W_R)\}$$

where \mathbf{R}^2 denotes the entire two-dimensional plane.

Given the value of $\tau_e = (\tau_X, \tau_Y)$ we redefine $(x_T, y_T) = (\tau_X, \tau_Y)$. Making (x_R, y_R) the integration variable running over $E(\omega_R)$ and setting

$$(x_S, y_S) = (I - M)^{-1} \left((x_T, y_T)^T - M(x_R, y_R)^T \right) \quad (3.20)$$

Equations (3.12 – 3.14) can be used to get

$$\begin{aligned}
 P\{\mathbf{W}_R \in E(\omega_R) \wedge \mathbf{W}_S \in E(\omega_S) \wedge \mathbf{T}_e = \tau_e\} = \\
 \int_{(x_R, y_R) \in E(\omega_R)} \left(\int_{(x_S, y_S) \in E(\omega_S)} \mu_R \mu_S \exp\left(-\frac{1}{2}(A_R(x_R, y_R) + A_S(x_S, y_S))\right) dx_S dy_S \right) dx_R dy_R = \\
 \mu_R \mu_S \int_{(x_R, y_R) \in E(\omega_R)} \exp\left(-\frac{1}{2}A_R(x_R, y_R)\right) \left(\int_{(x_S, y_S) \in E(\omega_S)} \exp\left(-\frac{1}{2}A_S(x_S, y_S)\right) dx_S dy_S \right) dx_R dy_R
 \end{aligned} \quad (3.20)$$

where

$$\mu_R \equiv \frac{1}{2\pi\sigma_{XR}\sigma_{YR}\sqrt{1-\rho_R^2}} \quad (3.21)$$

and a similar expression for μ_S , and where A_S and A_R are defined in Section 2.3.2.

Remark that (x_S, y_S) depends on (x_R, y_R) . Although the fact that \mathbf{C}_R and \mathbf{C}_S are symmetric matrices allows for several nice tricks (such as applying basis transformations), the second integral results in a complicated error-function expression. Instead of setting out on the heroic task of analytically integrating this error function (certainly prize winning if successful), we have chosen to determine this probability in a numerical way.

2.3.4.1 Alternative definition of probability of contact association

Remark that an alternative definition of the association probability in Equation (3.18) would be possible. It could also have been defined by

$$P\{\mathbf{W}_R \notin E(\omega_R) \wedge \mathbf{W}_S \notin E(\omega_S) \mid \mathbf{T}_e = \tau_e\}$$

what leads to an equal or smaller association probability. This choice cannot be made in one-dimensional situations, where a less likely value $W_R \geq \omega_R$ can only be combined with a value $W_S \leq \omega_S$ (also less likely than the actual observed value ω_S) if the condition $T_e = \tau_e$ must be met. For contacts in a 2-D plane, however, it is possible that a less likely R-contact position (\mathbf{W}_R outside the ellipse $E(\omega_R)$) has an associated value

$$\mathbf{W}_S = (\mathbf{I} - \mathbf{M})^{-1}(\tau_e - \mathbf{M} \cdot \mathbf{W}_R)$$

that is inside the ellipse $E(\omega_S)$ and is therefore more likely than ω_S . Here we have chosen to define a contact combination ($\mathbf{W}_R, \mathbf{W}_S$) less likely if at least one of those values is outside its pdf ellipse. This choice gives the highest association probability.

3 Understanding the association probability

All the relevant Equations presented in Chapter 2 are implemented in Matlab[®] to solve them numerically. It is worthwhile to analyse some outcomes to understand the processes that determine the association probability. First the successive steps for calculating the association probability are illustrated in Figure 3.1.

Thereafter the results of a carefully chosen set of contact situations are presented and compared with the one-dimensional solutions.

3.1 Visual presentation of the association probability

For the situation given in the lower right-hand panel of Figure 2.2, the upper left-hand panel of Figure 3.1 shows the contacts $\omega_R = (2050, 3000)$, $\omega_S = (2000, 3000)$ with the estimated target position $\tau_e = (2016.5, 3030.7)$ and the ellipses $E(\omega_R)$ and $E(\omega_S)$.

For all \mathbf{W}_R values inside $E(\omega_R)$ with $x_R = 1990$ the coupled \mathbf{W}_S values are calculated. Some of these \mathbf{W}_S values, however, are outside their $E(\omega_S)$ ellipse.

In the upper left-hand panel only those 27 combinations of \mathbf{W}_R and \mathbf{W}_S values are shown that are both inside their respective ellipses. For this reason some \mathbf{W}_R and \mathbf{W}_S values seem to be missing.

Each \mathbf{W}_R has a pdf value according to its bivariate normal distribution. Its coupled \mathbf{W}_S value has its own pdf value. The logarithm of these pdf values and the logarithm of their product are shown in the upper right-hand panel of Figure 3.1 for each of the 27 ($\mathbf{W}_R, \mathbf{W}_S$) combinations.

In the lower left-hand panel of Figure 3.1 for each possible \mathbf{W}_R position in the plane (whether inside or outside $E(\omega_R)$) the coupled \mathbf{W}_S value is determined and the product of their pdf values is assigned to the \mathbf{W}_R position. This shows the conditional probability densities for this specific case.

In the lower right-hand panel of Figure 3.1 all probability-density values for which the ($\mathbf{W}_R, \mathbf{W}_S$) combination is inside $E(\omega_R)$, respectively $E(\omega_S)$, are set equal to 0. The total probability density present in this panel (viz. $3.5e-5$) divided by the total probability density present in the lower left-hand panel (viz. $5.8e-5$) gives a probability of association of 0.60 for the contacts $\omega_R = (2050, 3000)$ and

$\omega_S = (2000, 3000)$ (for the numerical input values used: $\sigma_{xS} = 20$, $\sigma_{yS} = 40$, $\rho_S = 0.8$, $\sigma_{xR} = 40$, $\sigma_{yR} = 60$, $\rho_R = -0.8$).

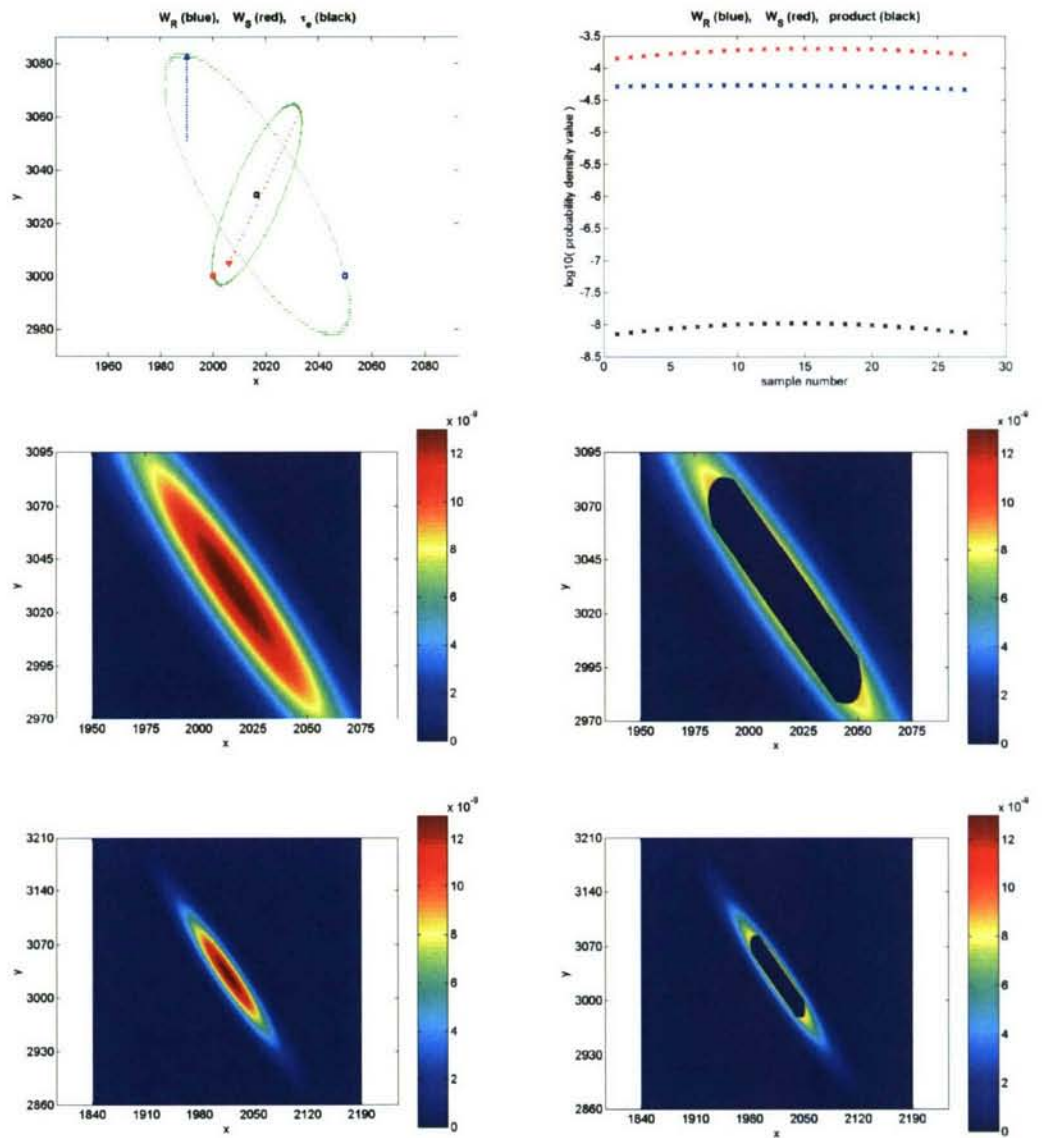


Figure 3.1 Upper left: the dots show the observations ω_R (blue) and ω_S (red) and the most-likely target position τ_e (black). The arrows show the coupling of W_R and W_S positions inside the ellipses $E(\omega_R)$ respectively $E(\omega_S)$. Upper right: probability density values of (W_R, W_S) combinations around τ_e . Middle and lower panels: colour maps of pdf-values contributing to probability of association: the probability equals the sum of the pdf-values in the right-hand panel divided by the same sum of the left-hand panel. The middle panels are a zoom of the lower panels, at the same scale as the upper left-hand panel.

3.2 Practical way to calculate the association probability

The above illustration suggests the following steps for the calculation of the association probability.

- 1 For a pair of observed contacts (ω_R, ω_S) determine the ML target position τ_e , using Equation (3.15).
- 2 Calculate the ellipses $E(\omega_R)$ and $E(\omega_S)$ from ω_R , ω_S and τ_e .
- 3 Choose a sufficiently large integration area around τ_e in the two-dimensional plane.

- 4 For each point \mathbf{W}_R in this integration area determine the accompanying \mathbf{W}_S position that combines with \mathbf{W}_R to $\mathbf{T}_e = \mathbf{T}_e$.
- 5 For each $(\mathbf{W}_R, \mathbf{W}_S)$ combination calculate the probability-density values $\text{pdf}(\mathbf{W}_R)$ and $\text{pdf}(\mathbf{W}_S)$, using Equation (3.12) and their product $p(\mathbf{W}_R) = \text{pdf}(\mathbf{W}_R) \cdot \text{pdf}(\mathbf{W}_S)$. In this way a 'probability density' value $p(\mathbf{W}_R)$ is assigned to each point \mathbf{W}_R in the integration area.
- 6 Integrate $p(\mathbf{W}_R)$ over the integration area.
- 7 Integrate $p(\mathbf{W}_R)$ over that part of $E(\omega_R)$ for which the accompanying \mathbf{W}_S values are also inside $E(\omega_S)$.
- 8 The association probability for the observed contact combination (ω_R, ω_S) is 1 minus (outcome of 7) divided by (outcome of 6).

3.3 Analysis of association probability

To study the mechanisms of the association process, a set of mutually comparable situations is considered. The contact positions are chosen as follows: In all cases $x_S = 2000$, $y_S = 3000$ and $y_R = 3000$. Only the x_R coordinate is varied, from $x_R = x_S + \sigma_{XR}/4$ (via $x_R = x_S + \sigma_{XR}/2$, $x_R = x_S + 3\sigma_{XR}/4$, $x_R = x_S + \sigma_{XR}$) to $x_R = x_S + 2\sigma_{XR}$.

For the distributions of the contacts the following choices are made:

- 1 $\sigma_{XR} = 2\sigma_{XS}$
- 2 $\sigma_{YR} = 2\sigma_{YS}$
- 3 either:
 - a $\rho_R = \rho_S = 0.8$ (so $\gamma = \delta = 0$ and \mathbf{T}_e on line with ω_R and ω_S)
 - b $\rho_R = -\rho_S$ and $\rho_S = 0.8$ (so $\gamma\delta \neq 0$ and \mathbf{T}_e is off line with ω_R and ω_S)

The values of σ_{XS} and σ_{YS} are varied (see Table 3.1). The first two choices mean that $\alpha = \beta$, see Section 2.3.3.

Table 3.1 summarises the results of this investigation. From this Table the following conclusions can be drawn:

- 1 The three cases $(\sigma_{XS} = 20, \sigma_{YS} = 40)$, $(\sigma_{XS} = 200, \sigma_{YS} = 4)$ and $(\sigma_{XS} = 2, \sigma_{YS} = 400)$ only differ by a scaling factor in both coordinate directions, but all calculated probabilities are exactly the same. Therefore it suffices to limit our attention to the first case $(\sigma_{XS} = 20, \sigma_{YS} = 40)$.
- 2 The association probabilities for differently oriented contact distributions (that is when $\rho_R = -\rho_S$ and so \mathbf{T}_e is not on the line between ω_R and ω_S) are much higher than for distributions with the same orientation.
- 3 For distributions with a different orientation ($\rho_R = -\rho_S$) the association probability is considerably higher than could be expected on the basis of a one dimensional analysis. But if both contact distributions have the same orientation ($\rho_R = \rho_S$) then the association probability is higher than the one-dimensional probability for two near contacts, but lower for two distant contacts. Further, $\rho_S = 0.8$ is a high value. For lower values of ρ_S the association probabilities in case both distributions have the same orientation ($\rho_R = \rho_S$) increase, but remain lower than for differently oriented distributions ($\rho_R = -\rho_S$).

To conclude, the more the distribution of the S contact differs from the distribution of the R contact, the more important the contribution of the two-dimensional analysis becomes.

Table 3.1 Results of associating two contacts with different parameters. See text above Table for details.

$x_R - x_S =$	τ_e on line between ω_R and ω_S ($\rho_R = \rho_S$)					τ_e not on line between ω_R and ω_S ($\rho_R = -\rho_S$)				
	$\sigma_{XR}/4$	$\sigma_{XR}/2$	$3\sigma_{XR}/4$	σ_{XR}	$2\sigma_{XR}$	$\sigma_{XR}/4$	$\sigma_{XR}/2$	$3\sigma_{XR}/4$	σ_{XR}	$2\sigma_{XR}$
$\sigma_{XS} = 20, \sigma_{YS} = 40$										
x_R	2010	2020	2030	2040	2080	2010	2020	2030	2040	2080
x_T	2002	2004	2006	2008	2016	2003.6	2007.2	2010.8	2014.4	2028.8
y_T	3000	3000	3000	3000	3000	3006.7	3013.3	3020	3026.6	3053.2
ass prob	0.93	0.76	0.54	0.33	0.01	0.98	0.91	0.82	0.69	0.24
1-dim prob	0.82	0.65	0.50	0.37	0.07	0.82	0.65	0.50	0.37	0.07
$\sigma_{XS} = 200, \sigma_{YS} = 4$										
x_R	2100	2200	2300	2400	2800	2100	2200	2300	2400	2800
x_T	2020	2040	2060	2080	2160	2036	2072	2108	2144	2288
y_T	3000	3000	3000	3000	3000	3000.7	3001.3	3002	3002.7	3005.3
ass prob	0.93	0.76	0.54	0.33	0.01	0.98	0.91	0.82	0.69	0.24
1-dim prob	0.82	0.65	0.50	0.37	0.07	0.82	0.65	0.50	0.37	0.07
$\sigma_{XS} = 2, \sigma_{YS} = 400$										
x_R	2001	2002	2003	2004	2008	2001	2002	2003	2004	2008
x_T	2000.2	2000.4	2000.6	2000.8	2001.6	2000.4	2000.7	2001.1	2001.4	2002.9
y_T	3000	3000	3000	3000	3000	3066.5	3133	3199.5	3266	3532
ass prob	0.93	0.76	0.54	0.33	0.01	0.98	0.91	0.82	0.69	0.24
1-dim prob	0.82	0.65	0.50	0.37	0.07	0.82	0.65	0.50	0.37	0.07

4 Performance estimation by means of simulations

4.1 Introduction

In order to study the consequences of the theory exposed in Section 2.3, and to evaluate different data-association rules, we have simulated two data sets, corresponding to the outputs of the two receiver systems S and R. The detection performance of S and R separately can then be compared to that of the combined system. This comparison is done using classical ROC curves.

Section 4.2 describes the simulations that are used for this analysis. In Section 4.2.3 the data-fusion algorithm is described in detail. Section 4.3 presents the simulated scenario. In Section 4.4 the results for the single sonars will be given. Sections 4.5 to 4.10 present the results after combining or fusing both data sets.

Before describing the simulations and their results, it is important to explain a few terms:

- 'detection' or 'contact': General threshold crossing.
- 'target': 'real' target inserted in the simulations.
- 'target detection': Threshold crossing corresponding to a 'real' target.
- 'false alarm': Threshold crossing not corresponding to a real target, but due to a statistical fluctuation of the background.
- 'combining' data sets: The contacts in the (two) original data sets are gathered in one list.
- 'fusing' data sets: The contacts in the (two) original data sets are gathered by applying a fusion algorithm to them and then making a list containing all contacts after this fusion.

'Combining' the data sets can thus be seen as 'fusing' them without any fusions to occur.

4.2 Simulations

4.2.1 Data-simulation procedure

In the simulations we have assumed two sonars to be present, a monostatic one (sonar 1) and a bistatic receiver (sonar 2). Both sonars are characterised by their position, and by a set of uncertainties in the following relevant quantities: sound speed, position, receiver heading, bearing estimates, time stamps.

These uncertainties represent the errors that are likely to be present in real sonar systems, as described e.g. in [1].

The simulations, used to assess the benefits of the data-association algorithm presented in the previous Chapters, are set up as follows:

- 1 General:
 - a Define the uncertainty in the sound speed (σ_c). This value is assumed to be equal for both sonars and constant over pings, and can be estimated from experience with sea-trial experiments.
 - b Two-dimensional propagation is assumed, i.e., no depth information is included.

- 2 Sonars:
 - a For sonar i ($i = 1, 2$) define its position $(x_{s,i}, y_{s,i})$.
 - b For each sonar, define the sampled beams.
 - c Define the sample frequency (assumed equal for both sonars) and the ping repetition rate. The latter defines the covered area for both sonars.
 - d For each sonar, generate sonar signals for each (range, bearing) cell. The sonar signals are intended to represent real sonar signals after beamforming and matched filtering, as in practice detection is applied after these two processing steps. The signals in the simulations are drawn randomly from a Rayleigh distribution, as this is the distribution that is most-often assumed to characterize real data.
 - e For sonar i ($i = 1, 2$), define the errors in:
 - i Position $(\sigma x_{s,i}, \sigma y_{s,i}, \sigma xy_{s,i})$.
 - ii Receiver heading $(\sigma \theta_i)$.
 - iii Bearing $(\sigma \phi_i)$.
 - iv Time synchronisation (σt_i) .
- 3 Targets:
 - a Define a number of targets n_t at fixed positions $(x_{t,j}, y_{t,j})$, $j = 1, \dots, n_t$.
 - b Define the target signal-to-noise ratios $SNR_{j,i}$ of target j with respect to sonar i . These signal-to-noise ratios relative to both sonars can be different due to the fact that both sonars see the target at a different aspect angle, for example.
 - c Determine the theoretical uncertainties $(\sigma x_{t,j}, \sigma y_{t,j}, \sigma xy_{t,j})$ in the target positions, based on $(\sigma c, \sigma x_{s,i}, \sigma y_{s,i}, \sigma xy_{s,i}, \sigma \theta_i, \sigma \phi_i, \sigma t_i)$. For this, the Equations of [3] are used. Note that the expected uncertainty in the target position will in general be different for sonars 1 and 2, as the parameters $(\sigma x_{s,i}, \sigma y_{s,i}, \sigma xy_{s,i}, \sigma \theta_i, \sigma \phi_i, \sigma t_i)$ themselves can be different for both sonars. In addition, the target will in general be at a different relative position relative to the sonars.
 - d For sonar i and for each ping p , generate an 'observed' target position $(x_{t,j,i,p}, y_{t,j,i,p})$ based on the true target position $(x_{t,j}, y_{t,j})$ and $(\sigma x_{t,i}, \sigma y_{t,i}, \sigma xy_{t,i})$.
- 4 Data:
 - a For both sonars and for each target, find the (range, bearing) cell $C_{t,j,p}$ that is closest to the 'observed' target position $(x_{t,j,i,p}, y_{t,j,i,p})$.
 - b At the cells $C_{t,j,p}$, generate new sonar signals with signal-to-noise ratio $SNR_{j,i}$.
 - c Take the logarithm of the data in every (range, bearing) cell.

4.2.2 Single-sonar detection procedure

After generating the data, as described in the previous Section, the detection performance of both single sonars is evaluated in the following way:

For both data sets i , apply amplitude thresholds A_T running from some low number (e.g. 9 dB) to some high number (e.g. 30 dB).

For each threshold A_T , count the number of threshold crossings in all cells $C_{t,j,p}$.

This number represents the number of target detections $N_{d,i,p}(A_T)$ for sonar i .

For each amplitude threshold A_T , count the total number of threshold crossings outside cells $C_{t,j,p}$. This number represents the number of false alarms, $N_{fa,i,p}(A_T)$ for sonar i .

The probabilities of detection and false alarm are determined by measuring, for each ping p , the number of detections $N_{d,i,p}(A_T)$ and false alarms $N_{fa,i,p}(A_T)$ as described above.

These numbers are then summed over all pings, which gives the total number of

detections and false alarms over all pings. These total numbers are then divided by their respective number of opportunities to have a threshold crossing. For the number of detections, $N_{d,i,p}(A_T)$, the number of opportunities is equal to the number of targets per ping times the number of pings. For the number of false alarms, $N_{fa,i,p}(A_T)$, the number of opportunities is equal to the number of (range, bearing)-cells minus the number of targets, times the number of pings.

In summary, the probabilities of detection and false alarm for sonar i ($i = 1, 2$) are determined via

$$p_{d,i}(A_T) = \frac{1}{N_{pings}} \frac{1}{\# \text{targets}} \sum_{p=1}^{N_{pings}} N_{d,i,p}(A_T) \quad (4.1)$$

$$p_{fa,i}(A_T) = \frac{1}{N_{pings}} \frac{1}{\#(\text{range, bearing}) \text{ cells} - \# \text{targets}} \sum_{p=1}^{N_{pings}} N_{fa,i,p}(A_T) \quad (4.2)$$

Plotting $p_{d,i}(A_T)$ versus $p_{fa,i}(A_T)$ generates a so-called ROC curve [6]. This is a well-known and well-accepted measure for estimating the sonar performance.

4.2.3 Data-fusion procedure

After having identified the two sets of threshold crossings, for every amplitude threshold, these two sets are fed to the fusion process. In practice, this fusion algorithm is implemented as follows:

- 1 The input data sets C_1 and C_2 consist of all contacts, above the relevant threshold, observed by sonar 1 and 2, respectively. Each contact in the data sets has seven labels:
 - a (x, y) , denoting the contact position (in metres).
 - b $(\sigma_x, \sigma_y, \sigma_{xy})$, indicating the expected uncertainty in the contact position (see Section 4.2.1).
 - c SNR , containing the mean contact signal-to-noise ratio.
 - d ID , a label that specifies if the contact is a false alarm ($ID = 0$), or corresponds to any of the targets ($ID = 1, \dots, n_t$).

To simplify things in the algorithm implementation, C_1 is assumed to contain not more elements than C_2 . If it does, C_1 and C_2 are interchanged.
- 2 Calculate the association probability between any pair of contacts from both data sets. The algorithms developed in Section 2.3 are used for this.
- 3 For each contact c_1 in data set C_1 , find the contact c_2 in data set C_2 for which the association probability P_{ass} is largest.
- 4 Check association by drawing a random number between 0 and 1. If this number is smaller than P_{ass} , the two contacts c_1 and c_2 are fused

- 5 Each contact that exists after the fusion process is passed to the output data set and has the following four labels:
 - a (x_f, y_f) , the ML contact position (in metres), as derived in Section 2.3.
 - b SNR_f , the mean contact SNR. For fused contacts it is the maximum of the two SNRs of the original contacts. For non-fused contacts it contains the SNR of the original contact.
 - c ID_f , a label that specifies the status and origin of the contact. The status can be:
 - i 'not fused'
 - ii 'fused'
- 6 For non-fused contacts the contact can originate from
 - i a true target
 - ii a false alarm
- 7 For fused contacts the contact can originate from:
 - i twice the same true target (e.g., target 2 as observed with sonar 1 and target 2 as observed with sonar 2).
 - ii two different true targets (e.g. target 3 as observed with sonar 1 and target 5 as observed with sonar 2).
 - iii a true target and a false alarm.
 - iv two false alarms.

It is necessary to keep track of all these possibilities to make sure that the data-fusion process does connect only valid pairs of contacts and not spurious close pairs.

There is one free parameter in the fusion process as we have implemented it: the size and shape of the covariance ellipses around the contact positions are used (see Section 2.3.2) to calculate the association probabilities. In principle, these ellipses should be the same as those that are used to generate the 'observed' target positions (see Section 4.2.1). However, we have allowed the ellipses used for the fusion process to be $F_{ellipse}$ times larger. The larger $F_{ellipse}$, the easier targets are associated. The introduction of this free parameter $F_{ellipse}$ seems somewhat ad hoc, but will turn out to be useful later on.

4.2.4 *Detection procedure after combining data sets*

After *combining* the two original sets of contacts, one data set remains that contains all contacts of the two original data sets. In this data set:

- True detections are identified as the true detections of the original data sets.
- False alarms are identified as the false alarms of the original data sets.

It should be ensured that, if a target is observed by both receivers, it is not counted twice as a true detection. That is, per ping the number of true detections can never exceed the number of targets present in the simulations.

This way of combining the data sets will be referred to as 'option 1' hereafter.

4.2.5 *Detection procedure after fusing data sets*

After *fusing* the two original sets of contacts, one data set remains. For this data set, we have defined different options which each have a different 'definition' of true detections and false alarms. These definitions are summarised in Table 4.1.

For example, in option 3 a contact after fusion is labelled a true target if it consists of either:

- A fused contact that originates from two identical true targets ($T_i T_i$).
- A (non-fused) contact that consists of a true target (T_i).
- A fused contact that originates from a true target and a false alarm ($T_i F$).
- A fused contact that originates from two non-identical true targets ($T_i T_k$).

Options 2 and 3 can be seen as variants of the 'OR' rule: if one of the receivers detects the target it is taken into account. Options 4 and 5 can be seen as variants the 'AND' rule: both receivers have to detect the target, and these two detections should fuse with each other.

For the labelled data, and for each amplitude threshold A_T , the numbers of true targets and false alarms with $\text{SNR} > A_T$ are then counted. For options 12 – 15 the numbers of true targets and false alarm with $\text{SNR} > A_T + \Delta A_T$ are counted.

Here ΔA_T is the increase in threshold that is applied, which is equal to the mean difference of the SNR of the fused contacts and the SNR of the original contacts that are fused. It serves to give non-fused contacts a lower detection probability relative to fused contacts. (Note that there is no physical justification for this, it is merely a heuristic way to try and improve the overall sonar performance after fusion).

Table 4.1 Different options to define true detections and false alarms after fusion. $T_i T_i$ denotes a fused contact that originates from two identical true targets. T_i denotes a true target that does not fuse. F denotes a false alarm that does not fuse. $T_i F$ denotes a fused contact that originates from a true target and a false alarm, $T_i T_k$ denotes a fused contact that originates from two non-identical true targets. FF denotes a fused contact that originates from two false alarms.

Option	True targets	False alarms	Amplitude threshold
data combining			
1	T_i	F	T
data fusing			
2	$T_i T_i, T_i$	$FF, F, T_i F, T_i T_k$	T
3	$T_i T_i, T_i, T_i F, T_i T_k$	FF, F	T
4	$T_i T_i$	$FF, T_i F, T_i T_k$	T
5	$T_i T_i, T_i F, T_i T_k$	FF	T
12	$T_i T_i, T_i$	$FF, F, T_i F, T_i T_k$	$T + \Delta T$
13	$T_i T_i, T_i, T_i F, T_i T_k$	FF, F	$T + \Delta T$
14	$T_i T_i$	$FF, T_i F, T_i T_k$	$T + \Delta T$
15	$T_i T_i, T_i F, T_i T_k$	FF	$T + \Delta T$

4.2.6 Presentation of results

For the single sonars 1 and 2, and for the combined data sets both with and without fusion, the ROC curves are generated and shown by plotting $p_{d,i}(A_T)$ versus $p_{fa,i}(A_T)$, and $p_{d,f}(A_T)$ versus $p_{fa,f}(A_T)$.

For the combined data set after fusion, the statistics of the fusion process are shown, i.e. the fraction of true detections and false alarms that are fused. Furthermore, the position parameters of the true detections are given, both before and after fusion, as this gives information on the improvement in target-position accuracy due to the fusion process.

4.3 Parameters of simulation scenario

For the simulations the following parameter values are chosen:

- Number of pings: $N_{pings} = 1000$
- Sample frequency: 100 Hz

- Ping-repetition rate: 10 s
- Sampled beams: -90 – 90 degrees, in steps of 2 degrees
- Sound speed: $c = 1500$ m/s
- St.dev. sound speed: $\sigma_c = 2$ m/s
- Position sonar 1: $(x_{s,1}, y_{s,1}) = (0, 0)$ m
- Position sonar 2: $(x_{s,2}, y_{s,2}) = (1000, 0)$ m
- St.dev. sonar positions: $(\sigma_{x_{s,i}}, \sigma_{y_{s,i}}, \sigma_{x_{y_{s,i}}}) = (20, 20, 0)$ m
- St.dev. receiver heading: $\sigma_{\theta_i} = 0.5$ degree
- St.dev. bearing estimate: $\sigma_{\phi_i} = 0.5$ degree
- Time error: $\sigma_{t_i} = 0.001$ s
- True position targets: random in observed area around both sonars
- Mean target SNR: 10 dB

Due to the non-zero beamspacing, and the low sample frequency (to save computation time), identified target detections will in general not be exactly at the true position of the target, but can be offset by up to 1.0 degree and about 7.5 m.

4.4 Single-sonar results

4.4.1 Checks on simulations

Before going into the possible benefits of data fusion, we check the data generation and the method to measure the ROC curves by calculating these curves for sonars 1 and 2 separately, and comparing these to the theoretically expected ROC curves.

Figure 4.1 shows the generated 'observed' target positions taken from bivariate normal distributions, using the true target position and the position covariances for both sonars. By comparing both panels in this Figure it is clear that the generated target positions are oriented differently due to the different shape and size of the covariance ellipses of both sonars. In this particular example, where only one true target is inserted, the positions are generated using the following covariance ellipses around the true target position:

- sonar 1:
 $\sigma_{x_{t,1}}$: 33.8 m
 $\sigma_{y_{t,1}}$: 30.1 m
- sonar 2:
 $\sigma_{x_{t,2}}$: 23.1 m
 $\sigma_{y_{t,2}}$: 24.3 m

The measured standard deviations of the 'observed' positions are:

- sonar 1:
 x -direction: 35.0 m
 y -direction: 29.1 m
- sonar 2:
 x -direction: 23.7 m
 y -direction: 24.8 m

The measured standard deviations are on average slightly larger than the standard deviations of the generated positions. This is because the 'observed' position of a target is the centre of the (range, bearing)-cell in which the generated position lies. As the generated position is usually not exactly in the centre of such a cell, this introduces a (small) extra scatter.

Figure 4.2 shows an example of the generated target positions if 10 targets are inserted in the simulations. This example serves to illustrate the fact that the size and shape of the covariance ellipses depend on the position of the target itself, as well as on the relative positions of the source and receiver sonars. The association probability will also depend on the position of the two contacts.

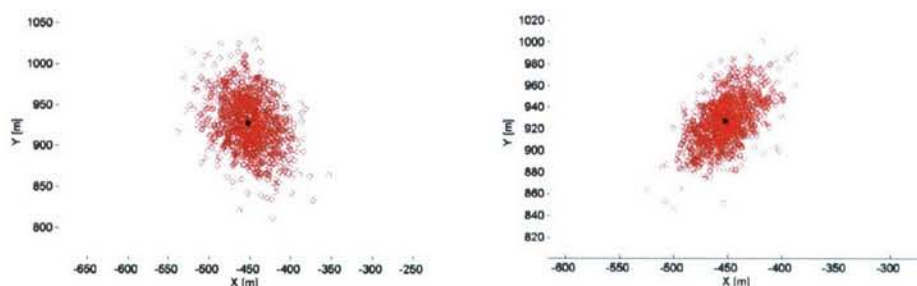


Figure 4.1 Example of generated erroneous target positions for sonar 1 (positioned at $(x, y) = (0, 0)$ m, assumed monostatic, left-hand panel) and sonar 2 (positioned at $(x, y) = (1000, 0)$ m, assumed bistatic, right-hand panel). One target is inserted in the simulations. Its true position is shown in black.

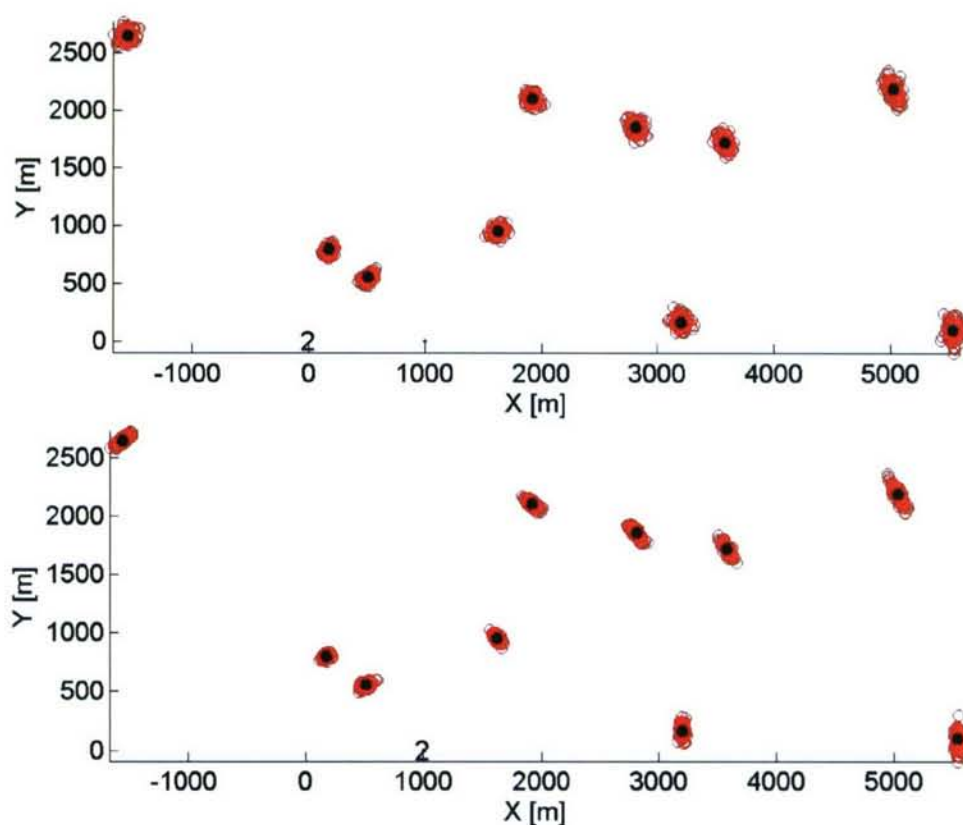


Figure 4.2 Example of generated erroneous target positions for sonar 1 (positioned at $(x, y) = (0, 0)$ m, assumed monostatic, top panel) and sonar 2 (positioned at $(x, y) = (1000, 0)$ m, assumed bistatic, bottom panel). Ten targets are inserted in the simulations. Their true positions are shown in black.

4.4.2 Detection performance

The detection results are shown in Figure 4.3 to Figure 4.5. Figure 4.3 shows the probabilities of detection, for both sonars, versus amplitude threshold. The measured values correspond very well with theory (black dashed curve). The theoretical curves are given by

$$P_{\text{det}} = \exp\left(-\frac{10^{A_T/10}}{2(1+snr)}\right) \quad (4.1)$$

(see e.g. Equation [9.4-14b] of [7]). Figure 4.4 shows the probabilities of false alarm versus amplitude threshold. Again, the measured values correspond very well with theoretical ones (black dashed curve), given by

$$P_{fa} = \exp\left(-\frac{10^{A_T/10}}{2}\right) \quad (4.2)$$

Figure 4.5 shows the ROC curves, i.e. the probability of detection versus the probability of false alarm. These also agree very well with the theoretical curves (black dashed lines), given by

$$P_{\text{det}} = P_{fa}^{1/(1+snr)} \quad (4.3)$$

Note that the ‘detection threshold’ DT , i.e. the signal-to-noise ratio for $P_d = 0.5$, can be derived from the amplitude threshold A_T according to

$$DT = 10^{10} \log\left(\frac{10 \log e}{10 \log 4} 10^{A_T/10} - 1\right) \quad (4.4)$$

Or

$$A_T = 10^{10} \log\left(\frac{10 \log 4}{10 \log e} (10^{DT/10} + 1)\right) \quad (4.5)$$

giving $A_T = 11.83$ dB if $DT = 10$.

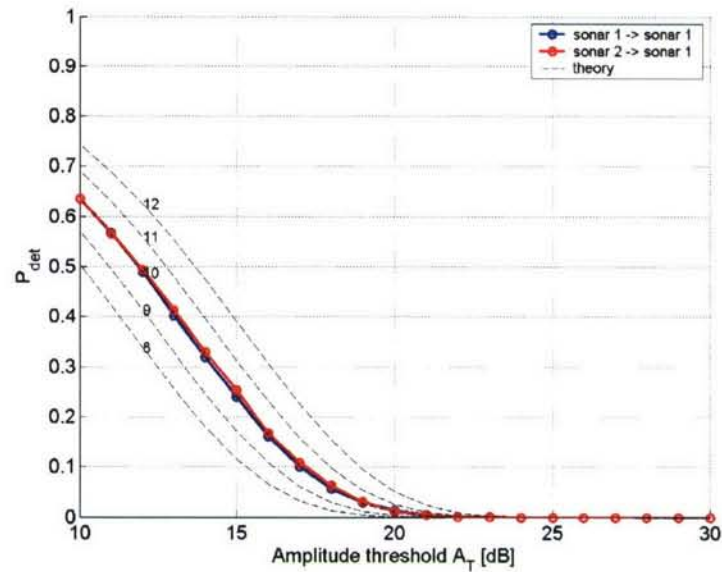


Figure 4.3 Simulated probability of detection for sonar 1 (blue) and 2 (red), for a mean target signal-to-noise ratio of 10 dB (relative to both sonars). The black dashed lines show the theoretical curves for different assumed SNRs (labels near curves, in dB) and Rayleigh statistics.

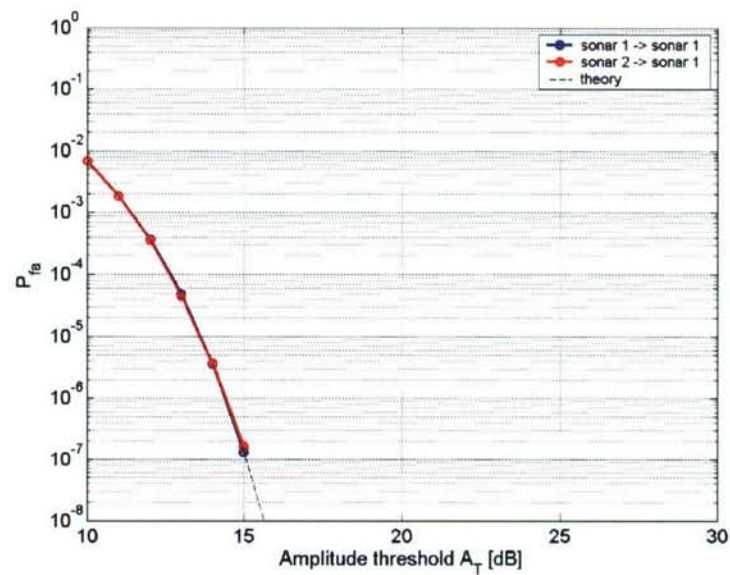


Figure 4.4 Simulated probability of false alarm for sonar 1 (blue) and 2 (red). The black dashed line shows the theoretical curve for Rayleigh statistics.

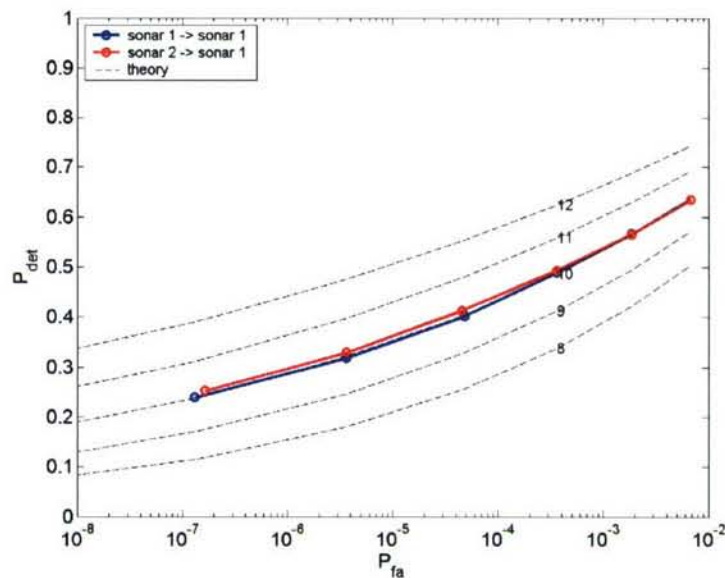


Figure 4.5 Simulated ROC curves for sonar 1 (blue) and 2 (red), for a target signal-to-noise ratio of 10 dB (relative to both sonars). The black dashed lines show the theoretical curves for different assumed SNRs (labels near curves, in dB) and Rayleigh statistics.

4.5 Statistics of fusions

Before showing the detection performance after fusion, we will first illustrate the fusion process itself by looking at its statistics. Figure 4.6 to Figure 4.11 show six examples of the fraction of detections that fuses, versus threshold. The difference between the examples is the following parameter values:

- Figure 4.6: target SNR: 10 dB, multiplication factor for position-error ellipses ($F_{ellipse}$): 1, number of targets: 1.
- Figure 4.7: target SNR: 10 dB, $F_{ellipse}$: 1, number of targets: 10.
- Figure 4.8: target SNR: 10 dB, $F_{ellipse}$: 1, number of targets: 30.
- Figure 4.9: target SNR: 10 dB, multiplication factor for position-error ellipses: 2, number of targets: 10.
- Figure 4.10: target SNR: 20 dB, $F_{ellipse}$: 1, number of targets: 10.
- Figure 4.11: target SNR: 20 dB, $F_{ellipse}$: 2, number of targets: 10.

In all Figures, we have made a subdivision into five classes:

- Fraction of false alarms that fuses with other false alarms (blue line).
- Fraction of false alarms that fuses with true detections (red line).
- Fraction of true detections that fuses with false alarms (green line).
- Fraction of true detections that fuses with true detections of other targets (e.g. a true detection of target 2 fuses with a true detection of target 5, black line).
- Fraction of true detections that fuses with true detections of the same target (magenta line).

From all Figures the following observations can be made:

- The fraction of false alarms that fuses with other false alarms (blue lines) decreases strongly with threshold. This is because the number of false alarms decreases strongly with threshold, and thus their mutual separation increases strongly, resulting in fewer fusions.

- The fraction of false alarms that fuses with true detections (red lines) is small, at most 1%. It is smaller than the fraction of false alarms that fuses with other false alarms. This is, of course, as there are fewer true detections than false alarms to fuse with.
- The fraction of true detections that fuses with false alarms (green lines) is about equal to the fraction of false alarms that fuses with other false alarms (blue lines). This is logical: these fusions are spurious fusions and their fraction is dominated by the density of false alarms.
(Note that this fraction is in principle the same as the previous one [fraction of false alarms that fuses with true detections], only scaled with the total number of true detections instead of with the total number of false alarms.)
- The fraction of true detections that fuses with other (but different) true detections (black lines) is very small, <1%. This is good news: it shows that, even if multiple targets are present in the data, fusions between target i in the first data set with target $j \neq i$ in the second data set are expected to occur not too often.
- The fraction of true detections that fuses with their counterpart in the other data set (magenta line) decreases with threshold. The reason for the decrease is that it is less likely that both sonars will 'detect' the target for higher threshold, and it is thus less likely that two observations of the same target will fuse.

In Figure 4.7 (mean target SNR = 10 dB, 10 targets) the fraction of true detections that fuses with their counterpart in the other data set is quite low, about 15%, even at low threshold. Apparently, the distance between the two observations of one target is too large to allow for a fusion fraction that is, say, more than 20%.

One 'solution' for this is to increase the size of the position-error ellipses for fusion with respect to that for the generation of the position errors (see Section 4.2.3).

This is illustrated in Figure 4.9, where the size of the position-error ellipses for the fusion process is twice as large as that for the generation of the erroneous target positions. The fraction of true detections that fuses with their counterpart in the other data set has increased to 25% at low thresholds.

The same observation can be made by comparing Figure 4.10 (multiplication factor for position-error ellipses: 1) and Figure 4.11 (multiplication factor for position-error ellipses: 2). In both Figures the target SNR is 20 dB, and 10 targets are inserted in the simulations. The maximum fraction of true fusions increases from 30% (Figure 4.10) to 50% (Figure 4.11).

From Figure 4.6 and Figure 4.8, which both have a target SNR of 10 dB and a multiplication factor for position-error ellipses equal to 1, it can be observed that the number of targets in the simulation (1 respectively 30) does not change significantly the fraction of true fusions, although this fraction increases slightly with the number of targets. It is to be expected that, only if the number of targets is similar to the number of false alarms, the number of spurious fusions between true targets and false alarms will increase, and the number of true fusions will thus decrease.

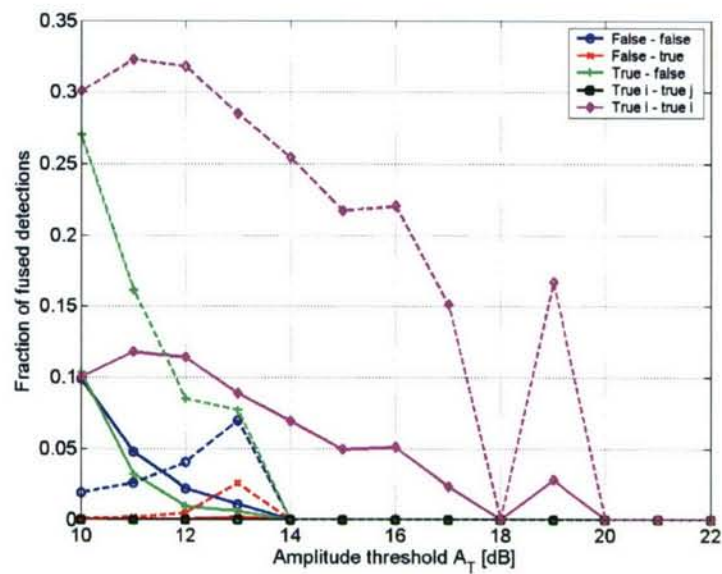


Figure 4.6 Fraction of detections that fuses, versus threshold. A target SNR of 10 dB is used, and 1 target is inserted in the simulations. The size of the position-error ellipses for the fusion process is equal to that for the generation of the erroneous target positions. Solid and dashed lines denote the mean values and standard deviations over all pings.

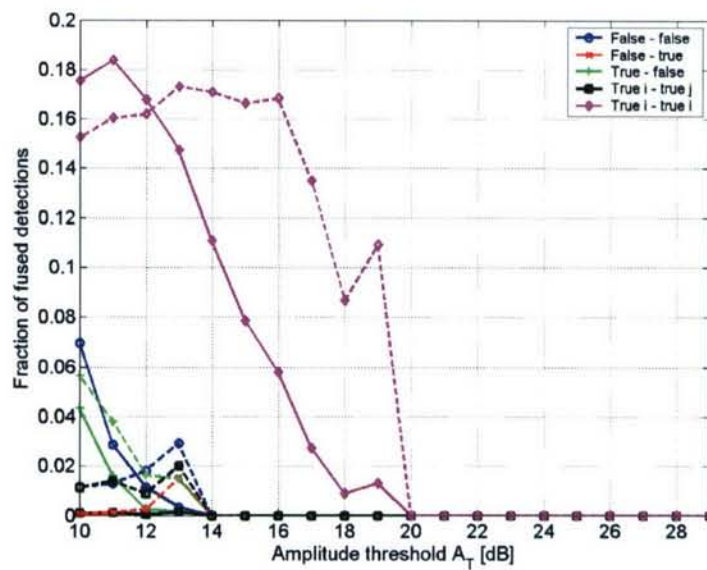


Figure 4.7 Fraction of detections that fuses, versus threshold. A target SNR of 10 dB is used, and 10 targets are inserted in the simulations. The size of the position-error ellipses for the fusion process is equal to that for the generation of the erroneous target positions. Solid and dashed lines denote the mean values and standard deviations over all pings.

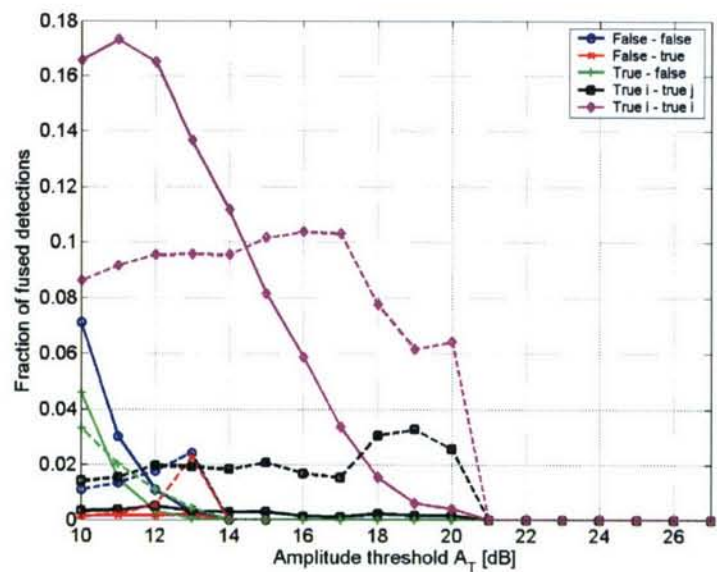


Figure 4.8 Fraction of detections that fuses, versus threshold. A target SNR of 10 dB is used, and 30 targets are inserted in the simulations. The size of the position-error ellipses for the fusion process is equal to that for the generation of the erroneous target positions. Solid and dashed lines denote the mean values and standard deviations over all pings.

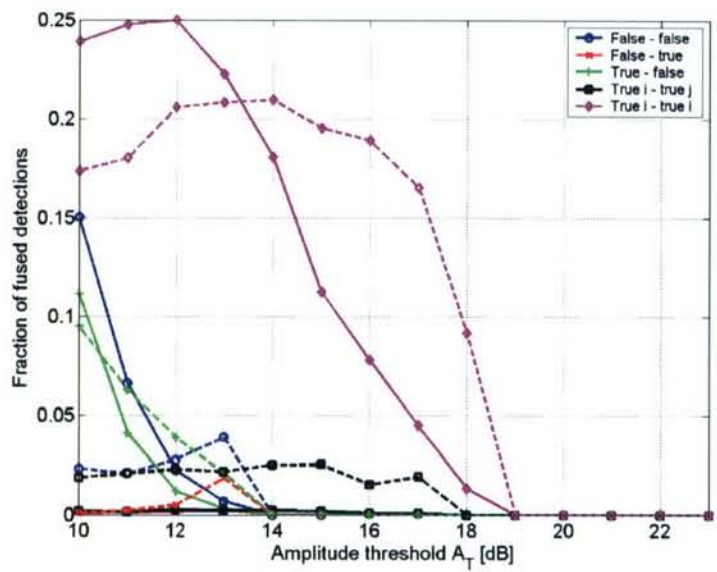


Figure 4.9 Fraction of detections that fuses, versus threshold. A target SNR of 10 dB is used, and 10 targets are inserted in the simulations. The size of the position-error ellipses for the fusion process is two times larger than for the generation of the erroneous target positions. Solid and dashed lines denote the mean values and standard deviations over all pings.

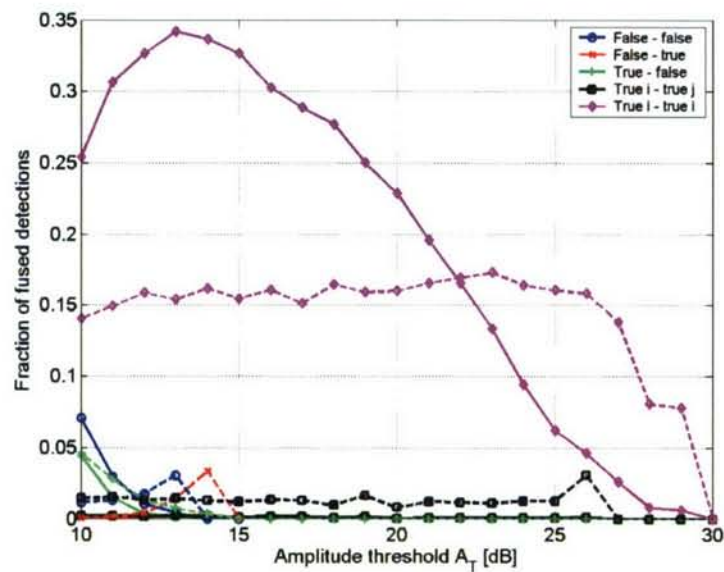


Figure 4.10 Fraction of detections that fuses, versus threshold. A target SNR of 20 dB is used, and 10 targets are inserted in the simulations. The size of the position-error ellipses for the fusion process is equal to that for the generation of the erroneous target positions. Solid and dashed lines denote the mean values and standard deviations over all pings.

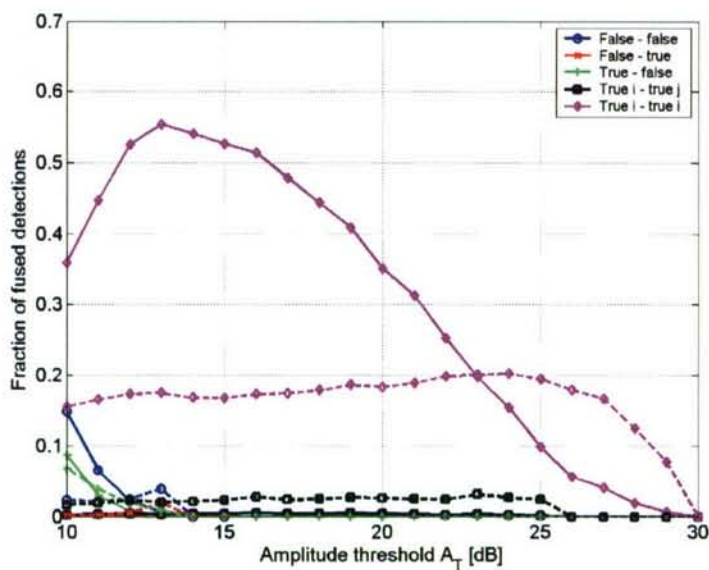


Figure 4.11 Fraction of detections that fuses, versus threshold. A target SNR of 20 dB is used, and 10 targets are inserted in the simulations. The size of the position-error ellipses for the fusion process is two times larger than that for the generation of the erroneous target positions. Solid and dashed lines denote the mean values and standard deviations over all pings.

4.6 Increase in amplitude threshold after fusion

As was mentioned in Section 4.2.5, we allow the option to increase the amplitude threshold based on the statistics of the fusion process. That is, when two contacts are fused, the SNR of the fused contact is set equal to the maximum of the two original contacts. This means that the mean SNR assigned to all fused contacts will be higher

than the mean original SNR of all contacts that are fused. This increase is denoted by ΔA_T . In order to give higher confidence to the fused contacts in the detection process, we can increase the amplitude threshold by ΔA_T , so that fewer non-fused contacts will pass the new threshold $A_T + \Delta A_T$.

Figure 4.12 shows ΔA_T versus A_T for the case where there are 10 targets, each with a mean SNR of 10 dB. It is clear from this Figure that at low thresholds ($A_T < 15$ dB) the increase in threshold is quite large, sometimes more than 1 dB. This means that instead of applying the nominal threshold of e.g. 11 dB, a threshold of 11.5 dB is applied. This will only occasionally affect the number of fused contacts that are detected, but it will decrease the number of non-fused contacts for that threshold.

It should be remarked that:

- ΔA_T is significantly larger for the fusion of true contacts than for the fusion of false contacts. This is because the mean SNR of the true contacts is 10 dB larger than the mean SNR of false alarms. With this higher mean SNR, the spread will also be larger.
- ΔA_T decreases with A_T for both categories. This is because the difference in SNR between both original contacts will decrease with A_T . Both contacts have to have an SNR larger than A_T , and the higher A_T , the smaller the difference in both SNRs.

The mean ΔA_T (blue line) increases between $A_T = 10$ and $A_T = 13$ dB, because the relative ratio of true – true and false – false fusions increases with A_T .

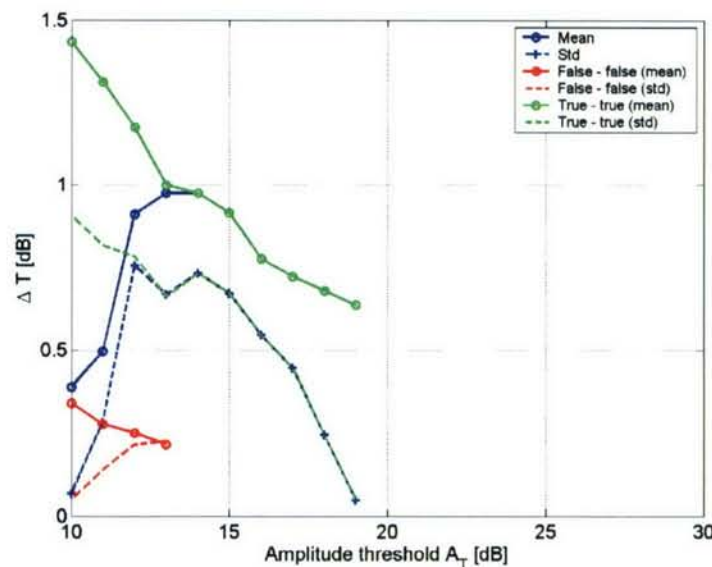


Figure 4.12 Increase in amplitude threshold, calculated from the mean difference in SNR before and after fusion (see text above Figure for details). Solid lines: mean increase in threshold over all pings, dashed lines: standard deviation. Red lines: only using false-alarm – false-alarm fusions, green line: only using true-detection – true-detection fusions, blue line: using all fusions.

4.7 False-alarm probability after fusion

Figure 4.13 shows the false-alarm probabilities after fusing the two data sets. The number of targets inserted in the simulations is 10, and their mean SNR is 10 dB. The size of the position-error ellipses for the fusion process is equal to that for

the generation of the erroneous target positions. The different options correspond to those in Table 4.1.

The following observations can be made from Figure 4.13:

- The false-alarm probabilities of the combined data set and for options 2, 12, and 3, are a factor two larger than that of the two separate sonars (as shown in Figure 4.4). This is because the total number of false alarms is *not* scaled with the total number of false-alarm opportunities in *both data sets*, but with the total number of false-alarm opportunities in one data set.
- The fall-off of the false alarm probability is the same as the theoretical curve (black dashed line) that is based on Rayleigh statistics. There is no reason for the fused contacts to follow this curve, but as there are more non-fused than fused contacts, the non-fused contacts dominate the statistics.
- The false-alarm probabilities for options 4, 14, 5 and 15 (i.e., only considering fused contacts) are a factor of 10 – 30 smaller than those for options 2, 12, 3 and 13 (which consider all contacts after fusion).
- The false-alarm probabilities for options 12 and 13 (i.e., above $A_T + \Delta A_T$) are roughly a factor of two smaller than those for option 2 and 3 (i.e., above A_T). The number of false alarms is thus decreased significantly by raising the amplitude threshold by ΔA_T .
- The false-alarm probabilities for options 14 and 15 (i.e., above $A_T + \Delta A_T$) are only slightly smaller than those for option 4 and 5 (i.e., above A_T). That is, the number of false alarms is not decreased significantly by raising the amplitude threshold if only fused contacts are considered.

For the influence of the number of targets inserted in the simulations, their mean SNR, and the size of the position-error ellipses on the false-alarm probabilities, see Section 4.10.

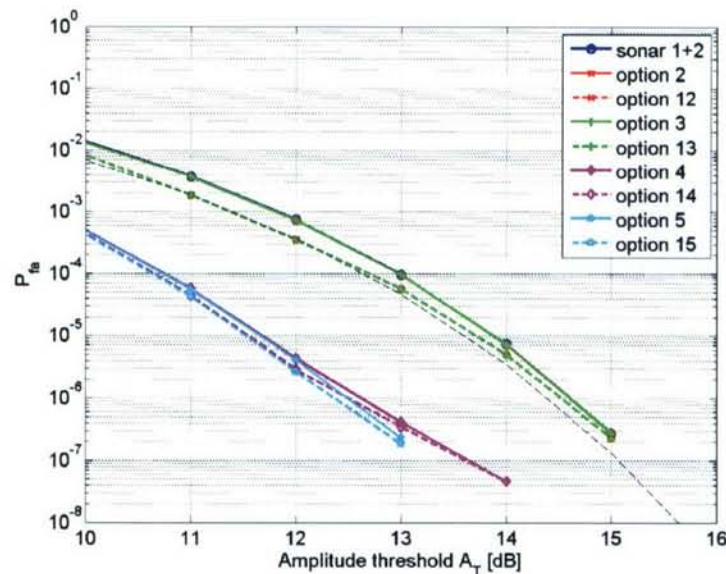


Figure 4.13 False-alarm probability for sonars 1 and 2 combined (blue solid line) and sonars 1 and 2 fused (other lines). The different options are explained in Table 4.1 (solid lines: 'OR' fusion, dashed lines: 'AND' fusion). The results for options 2 and 3 overlap, as well as those for options 12 and 13, for options 4 and 5 and for options 14 and 15. The black dashed line shows the theoretical curve for Rayleigh statistics.

4.8 Probability of detection after fusion

Figure 4.14 shows the probability of detection after fusing the two data sets. In both examples, the number of targets inserted in the simulations is 10, and their mean SNR is 10 dB. The size of the position-error ellipses for the fusion process is equal to that for the generation of the erroneous target positions. The different options correspond to those in Table 4.1. The following observations can be made from Figure 4.14:

- The probability of detection of the combined data set (blue solid line) is nearly equal to the theoretical value after 'OR' fusion,

$$P_{or} = 1 - (1 - P_1)(1 - P_2) \quad (4.6)$$

where P_i is the probability of detection of sonar i separately (black dotted lines). This is expected from theory, for two independent observations.

- The probabilities of detection for options 2, and 3 are almost equal to that of the combined data set. Those for options 12 and 13 are slightly smaller, about 0.02.
- The probabilities of detection for options 4, 14, 5 and 15 (i.e., only taking into account fused contacts) are much smaller than those of the combined data set, and a factor 2 – 3 smaller than the theoretical curves (black dashed lines). The latter is due to the small number of fusions that occurs (see Section 4.5), which results from the position errors on the single-sonar contacts. Without such position errors, more fusions would occur and the results would follow the theoretical lines much better.
- Including the increased threshold $A_T + \Delta A_T$ instead of A_T decreases the probability of detection by about 0.02.

For the influence of the number of targets inserted in the simulations, their mean SNR, and the size of the position-error ellipses on the probability of detection, see Section 4.10.

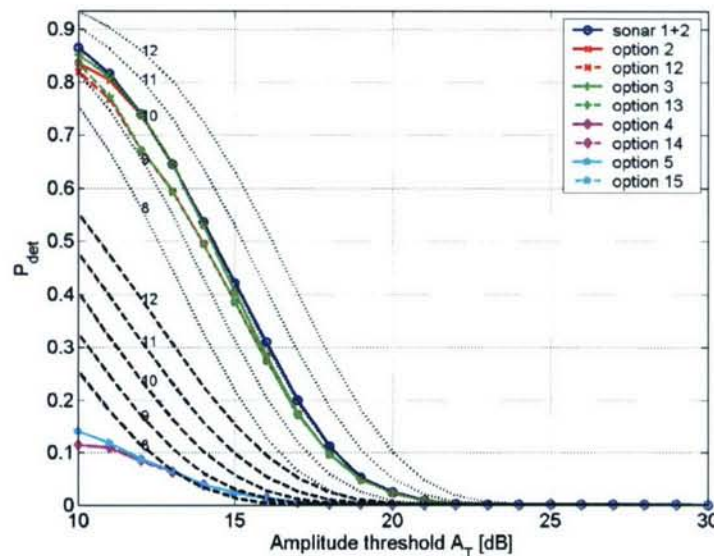


Figure 4.14 Probability of detection for sonars 1 and 2 combined (blue solid line) and sonars 1 and 2 fused. The different options are explained in Table 4.1 (solid lines: 'OR' fusion, dashed lines: 'AND' fusion). Black dotted lines: theoretical curves for 'OR' fusion and different assumed SNRs. Black dashed lines: theoretical curves for 'AND' fusion and different assumed SNRs.

4.9 ROC curves after fusion

Figure 4.15 shows the ROC curves after fusing the two data sets. In both examples, the number of targets inserted in the simulations is 10, and their mean SNR is 10 dB. The size of the position-error ellipses for the fusion process is equal to that for the generation of the erroneous target positions. The different options correspond to those in Table 4.1.

The following observations can be made from Figure 4.15:

- The operational SNR² of the combined data set (blue solid line) is significantly higher than that of the separate data sets (see Figure 4.16). This is a considerable performance improvement.
- The operational SNRs of the fused data sets with options 2, 12, 3 and 13 is also 1 – 5 dB higher than that of the separate data sets, and similar to that of the combined data set.
- The ROC curves for the combined data set and of the fused data sets with options 2, 12, 3 and 13 closely follow the theoretical ROC curves for the ‘OR’ fusion (black dotted lines). The theoretical ROC curves are obtained by plotting $1-(1-P_{det})^2$ versus $1-(1-P_{fa})^2$, where P_{det} and P_{fa} are given by Equations (4.1) and (4.2), respectively.
- The operational SNRs of the fused data sets with options 4, 14, 5 and 15 are much below that of the combined data set. The main reason is the small number of fusions that occurs (see Section 4.5), which is due to the position errors on the single-sonar contacts. Without such position errors, more fusions would occur.
- The ROC curves of the fused data sets with options 4, 14, 5 and 15 are reasonably close to the theoretical ROC curves for the ‘AND’ fusion (black dashed lines). The theoretical ROC curves are obtained by plotting P_{det}^2 versus P_{fa}^2 , where P_{det} and P_{fa} are given by Equations (4.1) and (4.2), respectively.

For the influence of the number of targets inserted in the simulations, their mean SNR, and the size of the position-error ellipses on the ROC curves, see Section 4.10.

² The operational SNR is usually defined as the SNR of the theoretical ROC curves that corresponds best to the data

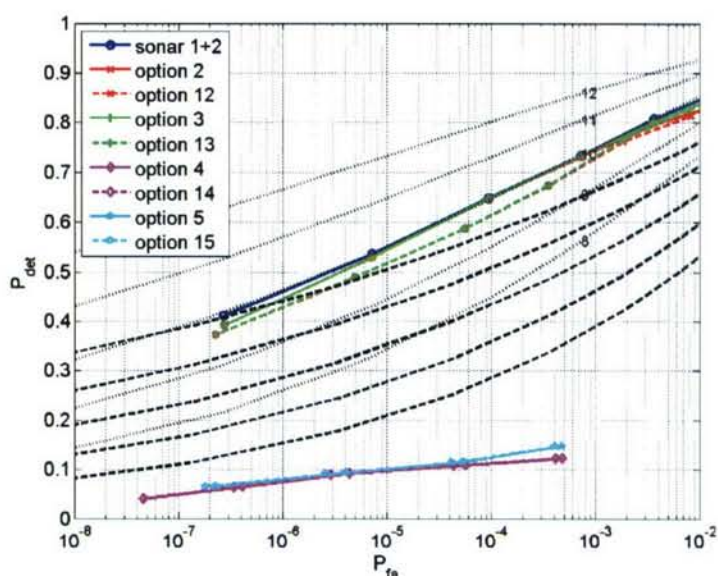


Figure 4.15 ROC curves for sonars 1 and 2 combined (blue solid line) and sonars 1 and 2 fused. The different options are explained in Table 4.1 (solid lines: 'OR' fusion, dashed lines: 'AND' fusion). 10 targets with mean SNR = 10 dB are inserted. Black dotted lines: theoretical curves for 'OR' fusion and different assumed SNRs. Black dashed lines: theoretical curves for 'AND' fusion and different assumed SNRs.

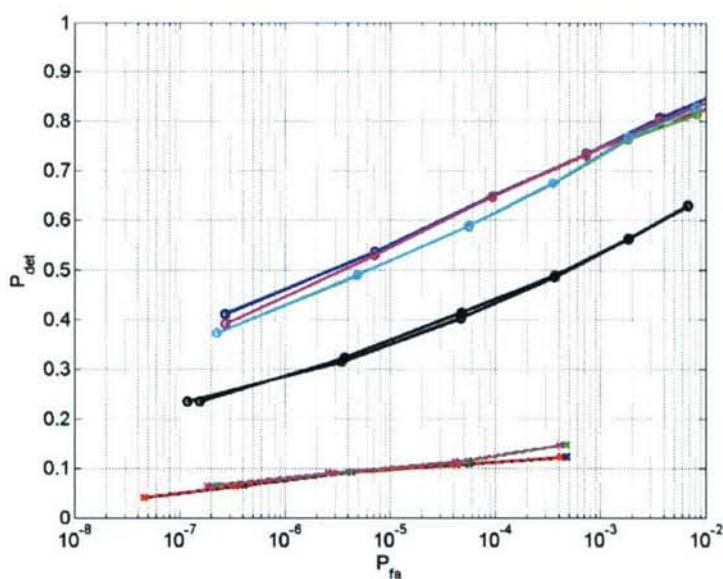


Figure 4.16 Comparison between single-sonar ROC curves (black lines) and ROC curves after combining or fusion the contacts (all other colors). 10 targets with mean SNR = 10 dB are inserted.

Summary

The above results can be summarised as follows:

Combining or 'OR' fusing two data sets, with a Rayleigh distribution for the target amplitudes, gives a considerable improvement of performance over using a single sonar. In hindsight this is to be expected and it can be derived from a proper theoretical analysis.

Using only the fused contacts ('AND' fusion), the false-alarm probability is very small, and reduces to almost zero for amplitude thresholds > 12 dB. However, the probability

of detection also reduces from about 0.6 to 0.1. This may be due to the low mean SNR of the target (10 dB in this case).

Using both the fused and non-fused contacts after fusion ('OR' fusion), the probability of detection and false alarm are roughly equal to those if the data sets are 'just' combined (i.e., with no fusion applied). 'OR' fusion thus does not seem to give much benefit over combining the two data sets. However, in Section 4.11 we will show that in some cases it may still be desirable to apply the fusion.

Before showing the benefits of fusion in Section 4.11, the next Section shows the ROC curves for different values of the input parameters of the simulation.

4.10 ROC curves for different simulation parameters

To study the dependence of the fusion on the input parameters of the simulation, we have varied the following parameters:

- Number of targets: 1, 3, 10, 30.
- Mean target SNR: 10, 15, 20 dB.
- Size of error ellipse used for fusion (see Section 4.2.3): 1, 2, 3 times larger than size of error ellipse used to generate the erroneous target positions.

Each of these three variations is treated in one of the following three Sections.

4.10.1 Number of targets

Figure 4.17 shows the ROC curves for different numbers of targets (1 and 30).

The mean target SNR is set to 10 dB, and the size of the error ellipses is equal to that used for generating the erroneous target positions. It is found that the number of targets inserted in the simulations does not significantly influence the false-alarm probabilities or the probability of detection, as is expected. A larger number of targets only leads to better statistics, but does not significantly increase the number of fusions between contacts that originate from different targets.

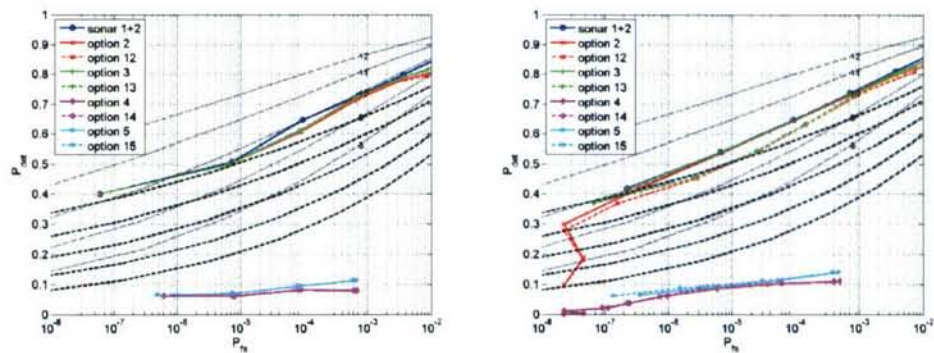


Figure 4.17 ROC curves for sonars 1 and 2 combined (blue solid line) and sonars 1 and 2 fused. The different options are explained in Table 4.1. Left: 1 target. Right: 30 targets. Black dotted lines: theoretical curves for 'OR' fusion and different assumed SNRs. Black dashed lines: theoretical curves for 'AND' fusion and different assumed SNRs.

4.10.2 Target SNR

It is found that the target SNR does influence the false-alarm probabilities if the mean SNR is quite high, e.g. 20 dB (see Figure 4.18). The reason for this is the fusion of target contacts with false alarms (T_iF option in Table 4.1). In fact, only about one such fusion in 100 simulations is enough to account for this.

The target SNR does influence the probability of detection quite strongly, as expected (see Figure 4.19). In this Figure the number of targets is 10, and the size of the error ellipses is equal to that used for generating the erroneous target positions. The curves for options 2, 12, 3, and 13 follow nicely the theoretical curves for 'OR' fusion.

The curves for options 4, 14, 5 and 15 are much lower than the theoretical curves for 'AND' fusion, due to the position errors in the original contacts.

Figure 4.20 shows the resulting ROC curves for different mean target SNRs (10 and 20 dB). The ROC curves for all options improve if the target SNR increases. For higher target SNR, the ROC curves deviate more and more from the theoretical curves and some of the curves show peculiar patterns. The reason for this is the relatively large false-alarm probabilities at high thresholds (see Figure 4.18).

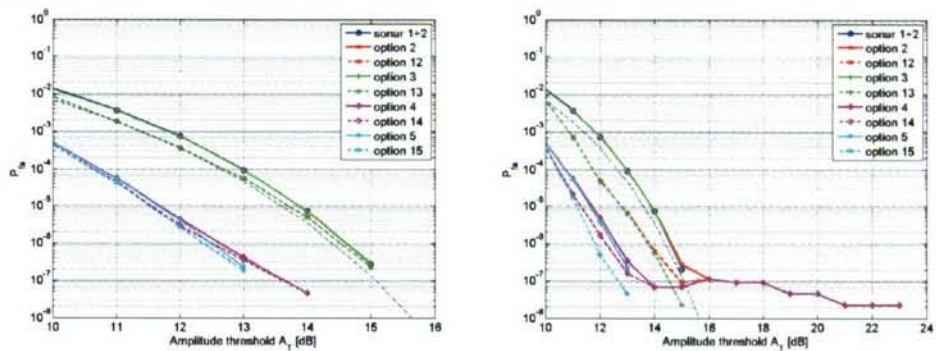


Figure 4.18 False-alarm probabilities for sonars 1 and 2 combined (blue solid line) and sonars 1 and 2 fused. The different options are explained in Table 4.1. Left: mean target SNR = 10 dB. Right: mean target SNR = 20 dB. Black dotted line: theoretical curve for Rayleigh statistics.

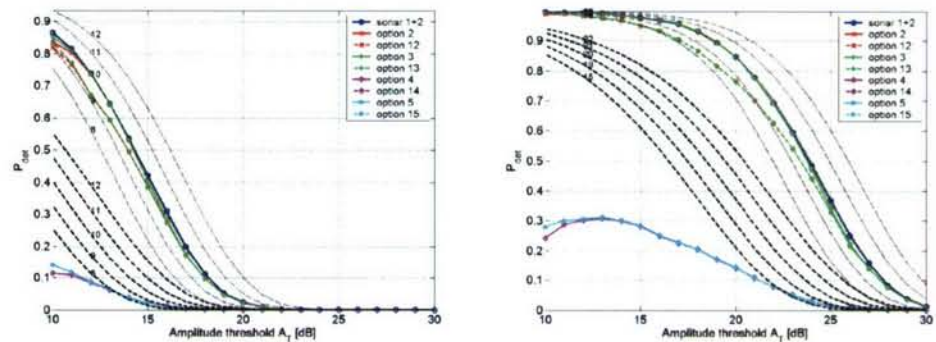


Figure 4.19 Probability of detection for sonars 1 and 2 combined (blue solid line) and sonars 1 and 2 fused. The different options are explained in Table 4.1. Left: mean target SNR = 10 dB. Right: mean target SNR = 20 dB. Black dotted lines: theoretical curves for 'OR' fusion and different assumed SNRs (see labels). Black dashed lines: theoretical curves for 'AND' fusion and different assumed SNRs (see labels).

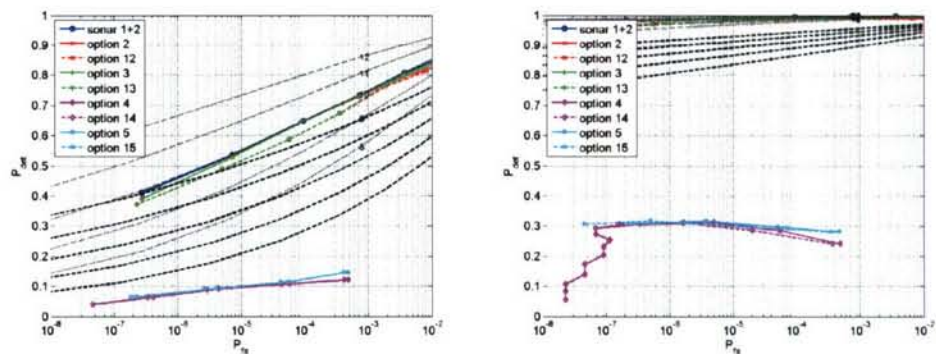


Figure 4.20 ROC curves for sonars 1 and 2 combined (blue solid line) and sonars 1 and 2 fused. The different options are explained in Table 4.1. Left: mean target SNR = 10 dB. Right: mean target SNR = 20 dB. Black dotted lines: theoretical curves for 'OR' fusion and different assumed SNRs (left: 8 – 12 dB, right: 15 – 20 dB). Black dashed lines: theoretical curves for 'AND' fusion and different assumed SNRs (left: 5 – 10 dB, right: 10 – 15 dB).

4.10.3 Size of error ellipse used for fusion

It is found that the size of the position-error ellipses for the fusion process does not significantly influence the false-alarm probabilities. Increasing the size of the position-error ellipses by a factor of 3 roughly doubles the probability of detection for options 4, 14, 5 and 15 (see Figure 4.21). In this Figure the number of targets is 10, and the target mean SNR is set to 10 dB. Figure 4.22 shows the corresponding ROC curves for different sizes of the error ellipses (factor 1 and 3 larger than error ellipse used to generate target positions).

The ROC curves only improve for options 4, 14, 5 and 15 (which all only include fused contacts), and mainly at lower amplitude thresholds. The reason for this is that it becomes easier for contacts to fuse.

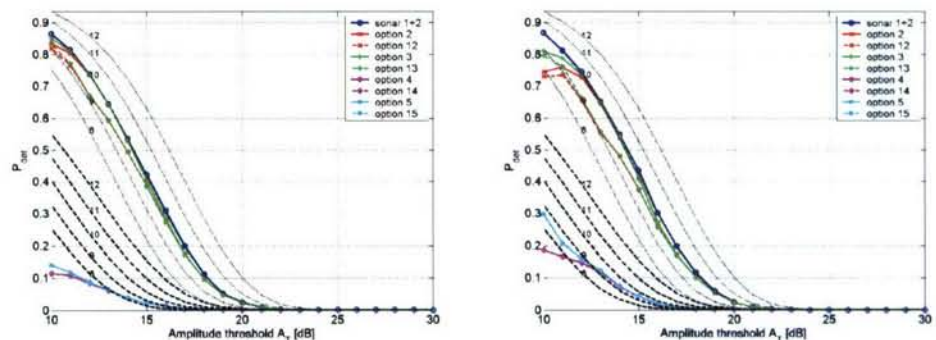


Figure 4.21 Probability of detection for sonars 1 and 2 combined (blue solid line) and sonars 1 and 2 fused. The different options are explained in Table 4.1. The size of the error ellipse used for fusion is a factor 1 (left) and 3 (right) larger than the size of the error ellipse used to generate the erroneous target positions. Black dotted lines: theoretical curves for 'OR' fusion and different assumed SNRs. Black dashed lines: theoretical curves for 'AND' fusion and different assumed SNRs.

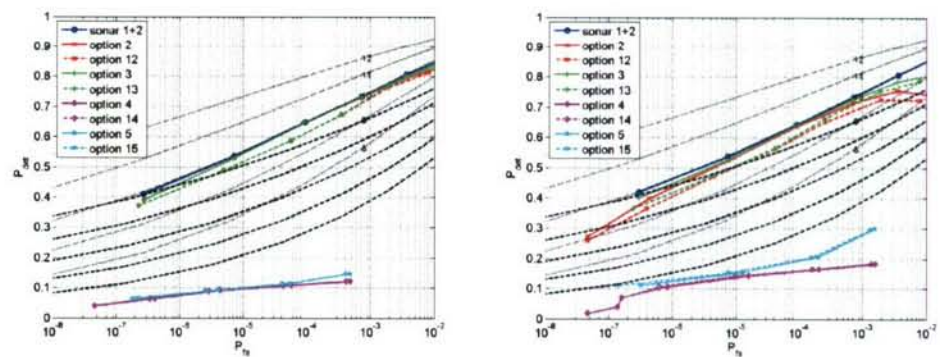


Figure 4.22 ROC curves for sonars 1 and 2 combined (blue solid line) and sonars 1 and 2 fused. The different options are explained in Table 4.1. The size of the error ellipse used for fusion is a factor 1 (left) and 3 (right) larger than the size of the error ellipse used to generate the erroneous target positions. Black dotted lines: theoretical curves for 'OR' fusion and different assumed SNRs. Black dashed lines: theoretical curves for 'AND' fusion and different assumed SNRs.

4.10.4 Target amplitude distribution

So far, a Rayleigh distribution was assumed for the background and for the target amplitude. This basically means that the fluctuations in the amplitude of both are random in nature. An alternative distribution, used for radar targets containing a strong highlight, is known as the one-dominant-plus-Rayleigh (1D+R) distribution [7]. We have evaluated the benefits of fusion with this 1D+R distribution as well, and compared it to the benefits of a Rayleigh distribution, see Figure 4.23. Although the ROC curves for both distributions are different, and the quantitative change due to fusion is different for both statistics, the overall improvement or decrease between the single-sonar performance (black lines) and that after fusion (lines in other colors) is similar for both situations.

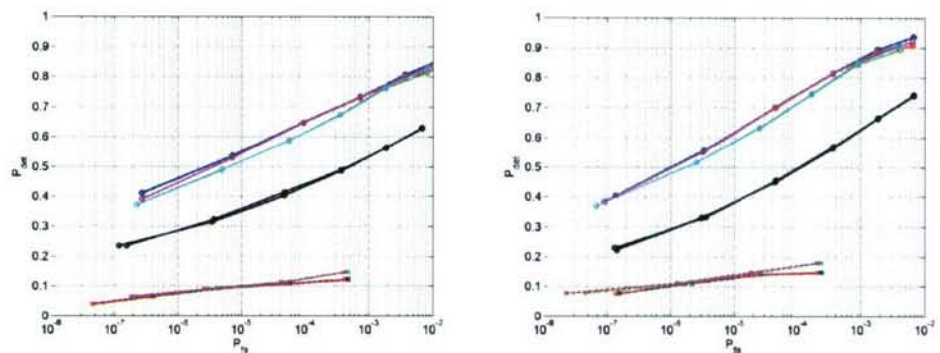


Figure 4.23 Comparison between single-sonar ROC curves (black lines) and ROC curves after combining or fusion the contacts (all other colors), using 10 targets with a mean SNR of 10 dB.
Left: Rayleigh distribution of target amplitude.
Right: One-dominant+Rayleigh distribution of target amplitude.

4.11 Improvement in localisation after fusion

The target detections with one sonar are usually observed at inaccurate positions (see also Section 4.4). Due to (small) errors in the sonar position, receiver heading, sound speed and time, the detections deviate from the true position of the target (see Figure 4.1 and Figure 4.2 for an illustration). Apart from the increase in detection

performance after fusion (see previous Sections), another benefit of fusing two (or more) data sets is the increased position information that one obtains for the targets. For the simulations with 30 targets inserted, this is illustrated in Table 4.2.

For sonars 1 and 2, 'Theory' gives the parameters of the covariance ellipses according to which the target positions are generated. 'Generated positions' refers to the positions where targets are placed in the simulations, given the errors in some fundamental parameters. These agree well with the theoretical values.

'Observed positions' refers to the position where the targets are observed, given the beam spacing and time sampling of the sonars. As explained in Section 4.4.1, these are slightly larger than the theoretical errors. This is because the observed position of a target is the centre of the (range, bearing)-cell in which the generated position lies. As the generated position is usually not exactly in the centre of such a cell, this introduces a (small) extra scatter.

The following remarks can be made from this Table:

- The mean offsets of the generated and observed positions of sonars 1 and 2 are always small, 1 – 3 metres.
- Using a fixed threshold of 10 dB, and evaluating fusion options 2, 12, 3 and 13, it can be witnessed that the standard deviations of the observed positions after fusion are similar to those before fusion. Most contacts included in these cases are non-fused contacts, which have the same position accuracy as those before fusion.
- Using a fixed threshold of 10 dB, and evaluating fusion options 4 and 14 (and to a lesser extent options 5 and 15), it can be witnessed that the standard deviations of the observed positions after fusion are smaller than those before fusion: the position estimate of contacts that originate from the fusion of two true contacts have a position accuracy that is roughly a factor 1.5 times better than that of the original contacts. This is an important observation that will, e.g. provide better input parameters for a tracking algorithm.
- For options 2 and 3 ('OR' fusion), the standard deviations of the observed positions decrease with threshold A_T , especially at higher thresholds, $A_T > 16$ dB. The standard deviations have roughly reduced to one third of their original value between $A_T = 10$ and $A_T = 20$ dB. This is because at higher threshold relatively more fused contacts are present, that have a higher position accuracy.
- For options 4 and 5 ('AND' fusion), the standard deviations of the observed positions also decreases with threshold A_T , the decrease being more profound at lower values of A_T than for options 2 and 3.

These results are found to be independent of the size of the error ellipses used for the fusion.

Table 4.2 Summary of position errors of generated and observed target positions relative to true target positions. All values are in metres and are mean values over 10 targets and 100 pings. N is the total number of contacts used in calculating the position errors.

	x-direction		y-direction	
	Mean	St.dev.	Mean	St.dev.
Sonar 1				
Theory	0	40	0	48
Generated positions	2	41	-2	49
Observed positions	2	45	1	54
Sonar 2				
Theory	0	33	0	39
Generated positions	-1	31	1	37
Observed positions	-2	35	3	44
After 'OR' fusion ($A_T = 10$ dB)				
Option 2 ($N = 1116$)	0	43	2	55
Option 12 ($N = 1078$)	0	42	3	56
Option 3 ($N = 1154$)	0	42	2	56
Option 13 ($N = 1116$)	0	42	3	56
After 'AND' fusion ($A_T = 10$ dB)				
Option 4 ($N = 128$)	0	23	1	34
Option 14 ($N = 128$)	0	23	1	34
Option 5 ($N = 193$)	0	30	-4	48
Option 15 ($N = 193$)	0	30	-4	48
After fusion (Option 2, 'OR')				
$A_T = 10$ dB ($N = 1116$)	0	42	2	55
$A_T = 12$ dB ($N = 869$)	0	40	3	52
$A_T = 14$ dB ($N = 589$)	-1	40	4	51
$A_T = 16$ dB ($N = 259$)	-1	36	5	47
$A_T = 18$ dB ($N = 85$)	0	28	4	30
$A_T = 20$ dB ($N = 24$)	-2	15	2	19
$A_T = 22$ dB ($N = 1$)	-1	0	1	0
After fusion (Option 3, 'OR')				
$A_T = 10$ dB ($N = 1154$)	0	42	2	56
$A_T = 12$ dB ($N = 869$)	0	39	3	51
$A_T = 14$ dB ($N = 589$)	-1	39	4	50
$A_T = 16$ dB ($N = 259$)	-1	35	5	45
$A_T = 18$ dB ($N = 85$)	0	25	3	27
$A_T = 20$ dB ($N = 24$)	-1	13	2	17
$A_T = 22$ dB ($N = 1$)	-1	0	0	0
After fusion (Option 4, 'AND')				
$A_T = 10$ dB ($N = 128$)	0	23	1	34
$A_T = 12$ dB ($N = 106$)	0	21	0	32
$A_T = 14$ dB ($N = 46$)	2	23	-2	27
$A_T = 16$ dB ($N = 9$)	-3	15	4	26
$A_T = 17$ dB ($N = 5$)	-5	12	5	21
After fusion (Option 5, 'AND')				
$A_T = 10$ dB ($N = 193$)	0	30	-4	48
$A_T = 12$ dB ($N = 106$)	0	21	0	32
$A_T = 14$ dB ($N = 46$)	2	23	-2	27
$A_T = 16$ dB ($N = 9$)	-3	15	4	26
$A_T = 17$ dB ($N = 5$)	-5	12	5	21

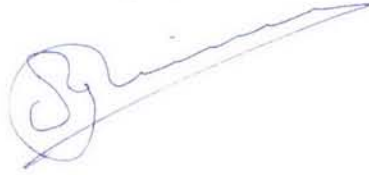
5 References

- [1] P.A.M. de Theije, J.C. Sindt,
Target localisation with multistatic systems,
UDT Asia, November 2003, Singapore.
- [2] P.A.M. de Theije, J.C. Sindt,
Single-ping target speed and course estimation using a bistatic sonar,
IEEE Journal of Oceanic Engineering, vol. 31, no. 1, p. 236, 2006.
- [3] S. Coraluppi,
Multistatic sonar localization analysis,
SACLANTCEN report, SR-377, June 2003.
- [4] S. Coraluppi,
Multistatic sonar localization analysis,
to appear in IEEE Journal of Oceanic Engineering, 2006.
- [5] D. Grimmer, S. Coraluppi,
Multistatic active sonar system interoperability, data fusion and measures of
performance,
NURC technical report, NURC-FR-2006-004, April 2006.
- [6] R.J. Urick,
Principles of Underwater Sound, 3rd edition, 1983.
- [7] J.V. DiFranco, W.L. Rubin,
Radar Detection,
Prentice-Hall, Englewood Cliffs, NJ, 1968.

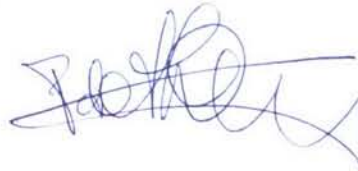
6 Signature

The Hague, December 2006

TNO Defence, Security and Safety

A handwritten signature in blue ink, consisting of a large, stylized 'D' followed by a long, sweeping horizontal line that extends to the right.

F.P.G. Driessen, MSc
Group leader

A handwritten signature in blue ink, featuring a complex, cursive style with multiple loops and a long, sweeping horizontal line at the end.

dr P.A.M. de Theije
Author

ONGERUBRICEERD
REPORT DOCUMENTATION PAGE
(MOD-NL)

1. DEFENCE REPORT NO (MOD-NL) TD2006-0178-	2. RECIPIENT'S ACCESSION NO -	3. PERFORMING ORGANIZATION REPORT NO TNO-DV 2006 A518
4. PROJECT/TASK/WORK UNIT NO 015.34675	5. CONTRACT NO V506	6. REPORT DATE December 2006
7. NUMBER OF PAGES 51 (excl RDP & distribution list)	8. NUMBER OF REFERENCES 7	9. TYPE OF REPORT AND DATES COVERED Final
10. TITLE AND SUBTITLE Algorithms for the fusion of two sets of (sonar) data		
11. AUTHOR(S) dr P.A.M. de Theije C.A.M. van Moll, MSc		
12. PERFORMING ORGANIZATION NAME(S) AND ADDRESS(ES) TNO Defence, Security and Safety, P.O. Box 96864, 2509 JG The Hague, The Netherlands Oude Waalsdorperweg 63, The Hague, The Netherlands		
13. SPONSORING AGENCY NAME(S) AND ADDRESS(ES) DMO/DWS&B/RZS/SWT, Royal Netherlands Navy, Van der Burchlaan 31, P.O. Box 90822, 2500 ES The Hague, The Netherlands		
14. SUPPLEMENTARY NOTES The classification designation Ongerubriceerd is equivalent to Unclassified, Stg. Confidentieel is equivalent to Confidential and Stg. Geheim is equivalent to Secret.		
15. ABSTRACT (MAXIMUM 200 WORDS (1044 BYTE)) <p>In this report we study different methods to combine sonar contacts as observed by two sonars. The sonar contacts are given realistic position errors, which makes their association non-trivial. First, for a single pair of contacts the most-likely position of the true underlying target position is derived. Based on this, the probability that two observed contacts originate from a single object is calculated. Based on these theoretical derivations, different association methods are evaluated using simulations, in which both targets-of-interest and false alarms are inserted. It is concluded that an 'OR'-fusion of the two sets of sonar contacts gives a much better performance than an 'AND'-fusion; the latter induces severe losses. The results are insensitive to the number of targets inserted, to the exact magnitude of the position errors, and to the amplitude distribution of the targets-of-interest.</p>		
16. DESCRIPTORS Sonar, data fusion, association, ROC curves		IDENTIFIERS
17a. SECURITY CLASSIFICATION (OF REPORT) Ongerubriceerd	17b. SECURITY CLASSIFICATION (OF PAGE) Ongerubriceerd	17c. SECURITY CLASSIFICATION (OF ABSTRACT) Ongerubriceerd
18. DISTRIBUTION AVAILABILITY STATEMENT Unlimited Distribution		17d. SECURITY CLASSIFICATION (OF TITLES) Ongerubriceerd

ONGERUBRICEERD

Distributionlist

Onderstaande instanties/personen ontvangen een volledig exemplaar van het rapport.

- | | |
|-------|---|
| 1 | DMO/SC-DR&D
standaard inclusief digitale versie bijgeleverd op cd-rom |
| 2/3 | DMO/DR&D/Kennistransfer |
| 4 | Programmabegeleider Defensie
ing. E. van de Spek
DMO/DWS&B/RZS&B |
| 5/7 | Bibliotheek KMA |
| 8 | TNO Defensie en Veiligheid, vestiging Den Haag,
Manager Waarnemingssystemen (operaties),
dr. M.W. Leeuw |
| 9 | Programmaleider TNO Defensie en Veiligheid
dr. S.P. Beerens |
| 10/11 | TNO Defensie en Veiligheid, vestiging Den Haag,
Archief |
| 12/18 | TNO Defensie en Veiligheid, vestiging Den Haag,
Business Unit Waarnemingssystemen,
ir. F.P.G. Driessen
ing. S.P. van Ijsselmuide
ir. C.A.M. van Moll
dr. P.A.M. de Theije
ir. W. Boek
dr. M.A. Ainslie
M.E.G.D. Colin |

Onderstaande instanties/personen ontvangen het managementuittreksel en de distributielijst van het rapport.

4 ex.	DMO/SC-DR&D
1 ex.	DMO/ressort Zeesystemen
1 ex.	DMO/ressort Landsystemen
1 ex.	DMO/ressort Luchtsystemen
2 ex.	BS/DS/DOBBP/SCOB
1 ex.	MIVD/AAR/BMT
1 ex.	Staf CZSK
1 ex.	Staf CLAS
1 ex.	Staf CLSK
1 ex.	Staf KMar
1 ex.	TNO Defensie en Veiligheid, Algemeen Directeur, ir. P.A.O.G. Korting
1 ex.	TNO Defensie en Veiligheid, Directie Directeur Operaties, ir. C. Eberwijn
1 ex.	TNO Defensie en Veiligheid, Directie Directeur Kennis, prof. dr. P. Werkhoven
1 ex.	TNO Defensie en Veiligheid, Directie Directeur Markt, G.D. Klein Baltink
1 ex.	TNO Defensie en Veiligheid, vestiging Den Haag, Manager Informatie en Operaties (operaties), drs. T. de Groot
1 ex.	TNO Defensie en Veiligheid, vestiging Rijswijk, daarna reserve Manager Bescherming, Munitie en Wapens (operaties), ir. P.J.M. Elands
1 ex.	TNO Defensie en Veiligheid, vestiging Rijswijk, Manager BC Bescherming (operaties), ir. R.J.A. Kersten
1 ex.	TNO Defensie en Veiligheid, vestiging Soesterberg, Manager Human Factors (operaties), drs. H.J. Vink